Probabilistic assessment of light water reactor fuel performance

Misfeldt, I.

Publication date:
1978

Document Version
Publisher's PDF, also known as Version of record

Risø Report No. 390

RISØ

Risø Report No. 390

Probabilistic Assessment of Light Water Reactor Fuel Performance

Ib Misfeldt

Risø National Laboratory, DK-4000 Roskilde, Denmark
October 1978

Risø Report No. 390

PROBABILISTIC ASSESSMENT OF LIGHT WATER REACTOR FUEL PERFORMANCE

Ib Misfeldt

Abstract. A computer system for the statistical evaluation of LWR fuel performance has been developed. The computer code FRP, Fuel Reliability Predictor, calculates the distributions for parameters characterizing the fuel performance and failure probability.

The statistical methods employed are either Monte Carlo simulations or a low order Taylor approximation.

Included in the computer system is a deterministic fuel performance code, which has been verified by comparison with data from irradiation experiments.

The distributions for all material data utilized in the fuel simulations are estimations from the best available information in the literature.

For the failure prediction, a stress corrosion failure creterion has been derived. The failure criterion is based on data from out-of-reactor stress corrosion experiments performed on unirradiated and irradiated zircaloy with iodine present.

October 1978
Risø National Laboratory, DK-4000 Roskilde, Denmark

By means of an example the typical distributions of the variables characterizing the fuel performance and the accuracy of the methods themselves have been investigated.

The application of the computer system is illustrated by a number of examples, these include the evaluation of irradiation experiments, design comparisons, and analyse of minor accidents.

INIS Descriptors BWR TYPE REACTORS, F CODES, FAILURES, FUEL PINS, IODINE, MONTE CARLO METHOD, PERFORMANCE, PROBABILITY, PWR TYPE REACTORS, RELIABILITY, STRESS CORRISION.

UDC (621.039.548.8 : 621.039.524.44) : 519.283

This report is submitted to the Technical University of Denmark, in partial fulfilment of the requirements for obtaining the lic. techn. (Ph.D.) degree.

ISBN 87-550-0586-1
ISSN 0418-6443

Risø Repro 1979

CONTENTS

		Page
1.	INTRODUCTION	5
2.	EVALUATION OF CONCEPTS	6
	2.1. Calculation of the fuel state, $\underline{Y}(t)$	8
	2.2. The probability of failure	10
3.	THE DETERMINISTIC FUEL MODEL, FFRS	13
	3.1. Stationary models for the regions	13
	3.2. The stationary solution for the fuel rod	15
	3.3. The time-dependent quasi-stationary model	16
	3.4. Verification of FFRS	18
4.	FUEL FAILURE CRITERIA	19
	4.1. Time-to-failure for stress corrosion	20
	4.2. Failure criteria under varying conditions	28
5.	MATERIAL AND DESIGN DATA	29
	5.1. Design data	29
	5.2. Material data	30
6.	NUMERICAL RESULTS FOR THE STATE VARIABLES	31
	6.1. Distribution of the state variables	33
	6.2. Accuracy of the Taylor approximation	40
	6.3. Calculations with reduced computer costs	44
7.	CALCULATIONS PERFORMED WITH FRP	45
	7.1. Failure probability for the two BWR designs	46
	7.2. Influence of the individual design and material parameters	50
8.	CONCLUSION	53
REFERENCES		54
APPENDIX A.	Specification of the numerical example used in chapter 6	56
APPENDIX B.	Typical applications of FRP; from reference 21	60

1. INTRODUCTION

The general performance of LWR fuel has been considerably improved in recent years, but problems with failures caused by pellet-cladding interactions (PCI) still exist and cause unscheduled shutdowns accompanied by serious economic consequences. The occurrence of PCI failures points to an effect which is attributed to statistical fluctuations, because they take place at power levels below that of the measured failure threshold in irradiation experiments. Therefore, the safety margins for the fuel are increased either by requiring a more stringent design or impose limitations on reactor operation (power levels, local ramp rates). Design specifications have been set rigidly, although no clear connection between these tolerances and fuel reliability with respect to the avoidance of PCI effects has yet been proved. The consequences of these restrictions on design and operation are increased fuel costs and reduced flexibility in the operation of nuclear power plants.

A probabilistic approach to fuel modeling provides information regarding the influence of tolerances on fuel reliability, as well as a quantitative basis for comparing designs and making improvements. The probabilistic approach seems, therefore, to provide a logical foundation for the evaluation of various designs.

For operating reactors, the probabilistic approach is expected to be a valuable tool for the establishment of optimal operational strategies, taking into account the cost of operational restrictions as well as that of fuel failures and design improvements.

The purpose of the work described in this report is to evaluate the failure probability for a nuclear fuel pin and to estimate the distribution of parameters required to characterize the fuel performance.

A nuclear fuel pin is a complex structural element, the performance of which depends on material properties, design specifications, and irradiation conditions. Therefore, a major effort was concentrated on the developing of a model of fuel-pin performance and the establishment of statistical models for the material properties of the fuel and cladding.

The time-dependent irradiation conditions are in general stochastic processes; in order to avoid any restrictions on the specified irradiation conditions, Monte Carlo simulations were chosen for the statistical method. In cases where the irradiation conditions can be expressed through deterministic functions and continuous stochastic variables, a Taylor expansion can be used to estimate the failure probability and the distribution of the parameters characterizing fuel performance. In this case the individual contributions from the stochastic variables used in the material equations, the design and irradiation specifications, also can be evaluated.

Typical distribution functions for the parameters characterizing the fuel performance are calculated and the truncation error of the Taylor expansion is investigated through comparisons with Monte Carlo simulations.

Finally, several examples illustrating the applications of the probabilistic approach are given.

2. EVALUATION OF CONCEPTS

A nuclear fuel pin is a complex structural element, and its behaviour cannot be satisfactorily modelled by means of a simple analytical approach. Therefore fuel pin behaviour is simulated by a computer code.

The statistical variation of fuel pin behaviour results from different factors such as statistical uncertainty on material behaviour, tolerances on dimensions, and uncertainty with respect to the applied load on the fuel pin.

Figure 2.1 shows a plan over the Fuel Reliability Predictor (FRP). Based on the applied load, $\underline{H}(t)$, and the design and material data, $\underline{X}$, FRP calculated the fuel state, $\underline{Y}(t)$, (distribution of temperature, strain, stress, etc., in pellet and cladding as function of time), and the failure probability for different failure criteria as a function of time, $\underline{W}(t)$.

The deterministic fuel model and the failure model are developed independently of the statistical model. Hence these models can be verified by means of relatively few irradiation experiments, as well as by comparison with the results obtained by other fuel models.

In principle, the input power history (applied load), $\underline{H}(t)$, is a stochastic process. However, for most applications it can be simplified to a deterministic function of time, h(t), with possible dependence on some stochastic variables.

Design and material data are stochastic variables characterized by probability density functions (pdf's) derived from experimental data.

The fuel state, $\underline{Y}(t)$, and the failure probability, $\underline{W}(t)$, are stochastic processes.

The deterministic fuel model, FFRS, the failure model, and the estimation of pdf's for material and design data are described in Chapters 3, 4 and 5, respectively.

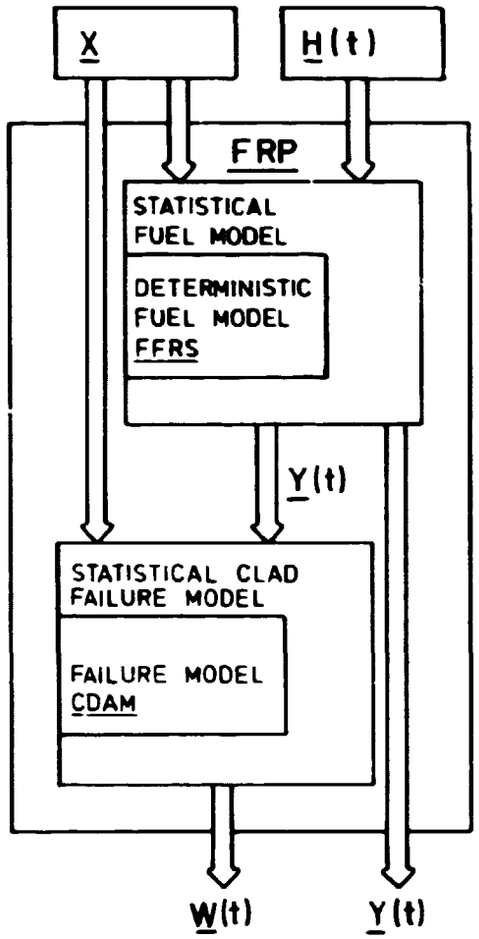

X: design and material data, stochastic variables.

H(t): applied load on the fuel (power, flux, etc.), stochastic process or a deterministic function of time.

Y(t): fuel state (stress, strain, etc.), stochastic process.

W(t): clad failures (stress corrosion, overstrain, etc.), stochastic process.

Fig. 2.1. The Fuel Reliability Predictor

2.1. Calculation of the fuel state, Y(t)

If the load is a general stochastic process, the only method applicable for the calculation of an approximation to the fuel state is a Monte Carlo simulation. This is a computation of a number of values from Y(t), each based on a new random sample from X and H(t). If the number of samples is large, the calculated values y(t) form a good approximation to Y(t).

2.1.1. Stochastic state variables, $\underline{Z}$

Calculation of the fuel state is restricted generally to some end-of-life and some extreme set of values, $\underline{Z}$. For example, these are the cladding permanent strain, the amount of released fission gas, and the maximum stress during irradiation. These stochastic variables provide sufficient information, in general, to describe the fuel state at any time. In this way, the problem of calculating the fuel state is reduced to that of calculating several stochastic variables. The pdf's for these variables can be approximated by Monte Carlo simulation to the accuracy required.

If the applied load were a deterministic function of time, h(t), instead of a function described by a stochastic process, the stochastic state variables would be functions of the design and material data alone.

$\underline{Z} = \underline{F}(\underline{X})$; $\underline{h}(t)$ a given deterministic function of time

If the applied load can be characterized by a deterministic function and a limited number of stochastic variables, these variables can be included in $\underline{X}$.

If the range of variables, X_i, are continuous random variables, the moments for the continuous values for $\underline{Z}$ can be approximated by a Taylor expansion. By retaining the terms up to the second order and assuming uncorrelated variables, the expression for the mean value and the variance for Z_i can be expressed, according to Hahn and Shapiro[1], as

$$\text{Mean } (Z_i) \equiv \bar{Z}_i = F_i(\underline{\bar{X}}) + \tfrac{1}{2} \sum_{j=1}^{n} \frac{\partial^2 F_i(\underline{\bar{X}})}{\partial X_j^2} \cdot \text{Var}(X_j)$$

$$\text{Var}(Z_i) = \sum_{j=1}^{n} \left(\frac{\partial F_i(\underline{\bar{X}})}{\partial X_j}\right)^2 \cdot \text{Var}(X_j) \qquad (2.1)$$

where $F_i(\underline{\bar{X}})$ is the ith state variable calculated by the deterministic fuel model, when all X_j's are at their mean values,

and n is the number of independent variables, X_j. The partial derivatives are evaluated numerically.

One major advantage of the Taylor approximation is the separately calculated contributions to the variance. They give useful information on the relative importance of the variables X_i. However, as the variance for some of the parameters is large, the accuracy of the approximation can be quite poor.

2.2. The probability of failure

The probability of failure of a system or structure is the likelihood of the occurrence of some unfavourable state, defined through a failure criterion.

In structural reliability, failure is normally defined as a condition in which the load exceeds the resistance of the structure. The resistance is a measure of the capability of the structure in meeting the demands.

2.2.1. Static load and resistance

If the load, L, and the resistance, R, are stochastic variables with probability density functions, $f_L(\ell)$ and $f_R(r)$, and the failure criterion is R < L, the probability of failure is

$$p(\text{failure}) = P(R < L) = \int_0^\infty \left[\int_0^\ell f_R(r)dr\right] f_L(\ell)d\ell$$

$$= \int_0^\infty F_R(\ell)\ f_L(\ell)d\ell \qquad (2.2)$$

where $F_R(r)$ is the cumulative distribution function for the resistance. The value corresponds to the area shown in Fig. 2.2.

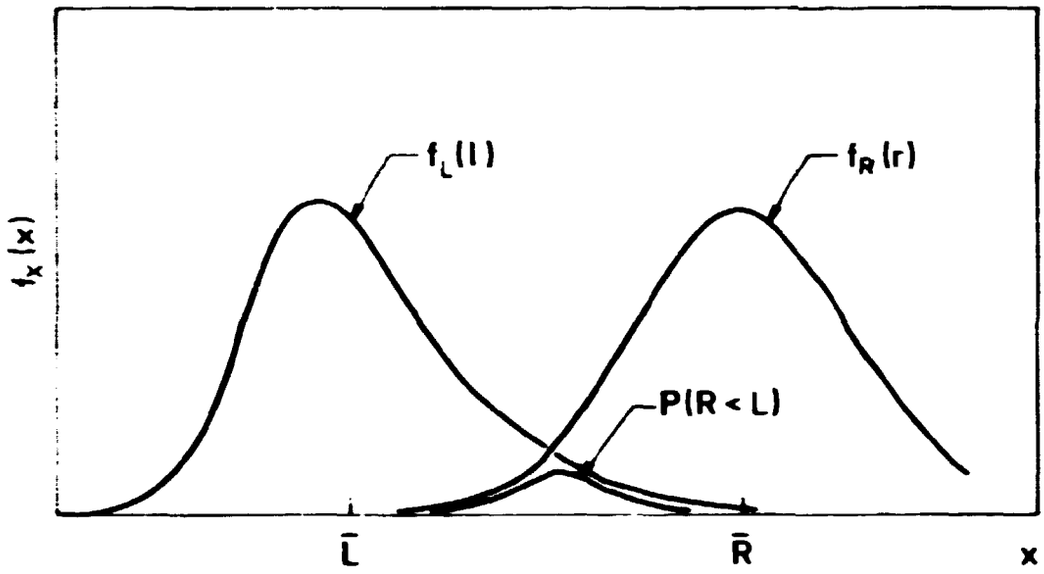

Fig. 2.2. Probability of failure

For a fuel rod, the fuel state, $\underline{Y}(t)$, or the state variables $\underline{Z}$ are functions of the power history, $\underline{H}(t)$, and the material and design data, $\underline{X}$. When evaluating the failure probability for a specific failure mode, some of the state processes or the state variables might be considered as a simplified load or resistance.

If the simplified load and resistance are independent stochastic variables, the failure probability can be evaluated according to 2.2, where the pdf's for the load and the resistance can be approximated by Monte Carlo approximation or Taylor expansion. One example in which this approach is used is described in ref. 2. The failure mode considered in this example is overstrain, with the strain-to-failure (the strain at which failure occurs) defined from tests on irradiated tubes. The load is defined as the tensile strain during the end-of-life ramp for the fuel rod. The embrittlement of the cladding is assumed saturated at the time of the ramp and therefore the resistance can be assumed independent of $\underline{H}(t)$ and $\underline{X}$.

For most failure modes, both load and resistance depend on the power history, in which case the failure probability cannot be evaluated according to 2.2. However, it is often possible to define a normalized load and resistance in such a way that the normalized resistance is independent of the irradiation (the power history), and the load is a stochastic variable.

This can be illustrated by an example where the strain in the end-of-life ramp is considered to be the dominating load. If the resistance (the strain to failure) is a function of neutron exposure (called fluence, ψ), $R = f(\psi) \cdot R'$, where R' is the unirradiated strain-to-failure (a stochastic variable) and f(fluence) is a deterministic function of the fluence, then the normalized load can be defined as

$$L' = L/f(\psi),$$

where L is the actual strain during the ramp and fluence is the neutron exposure at the time of the ramp. R' is the normalized resistance.

The failure probability can then be calculated according to 2.2 with the resistance R' and the load L'. L' and R' are independent stochastic variables and can be included in $\underline{Z}$.

For time-dependent failure modes, an analogous approach can be used, assuming for example that the failure process is cumulative as described for stress corrosion in Chapter 4.

2.2.2. The reliability index

Only if the pdf's for both R and L are known, the probability of failure $P(R-L<0)$ can be evaluated according to 2.2. If a Taylor expansion is used to obtain information regarding R and L, it is necessary to assume the pdf's on the basis of the calculated moments. Even if the Monte Carlo simulation is used, the failure probability often depends strongly on the tails of the pdf's of R and L; these in turn again depend on the tails of the pdf's for the variables in $\underline{X}$. These tails will seldom be known very accurately. Therefore the exact value for the failure probability is often unattainable; in this case the available information regarding the reliability instead should be expressed by a reliability index, β. This is defined by A.M. Hasofer and N.C. Lind[3] as the distance from the mean point (the point where all variables are at their mean values) to the failure region, where all variables are measured in standard deviation units.

If the failure criterion is $F<0$, where $F=R-L$ and R, L are normally distributed with mean $\bar{R}$, $\bar{L}$ and standard deviation s_R, s_L, respectively, the mean and standard deviation of F are respectively

$$\bar{F} = \bar{R} - \bar{L}, \quad s_F = \sqrt{s_R^2 + s_L^2} .$$

By making use of the above definition for a single variable, the reliability index is

$$\beta = \frac{\bar{F}}{s_F} = \frac{\bar{R} - \bar{L}}{\sqrt{s_R^2 + s_L^2}} . \qquad (2.3)$$

This expression is identical to the first-order Taylor approximation to β for any continuous distribution of R and L.

3. THE DETERMINISTIC FUEL MODEL, FFRS

FFRS was developed for use in FRP; therefore the code should be fast (in computer time) and it should respond correctly to reasonable changes in design data, material data and operational conditions.

A short description of the model is given below; a more comprehensive description is found in ref. 4.

Only a slice (dics) of the fuel is treated in the model, except in the case of fission gas release and internal pressure where an approximation to the whole rod is used. The slice is divided into three regions: cladding, gap, and fuel. The fuel is subdivided by a bridging annulus into a rigid, totally cracked zone and a perfectly plastic zone.

3.1. Stationary models for the regions

The cladding is treated as an axisymmetric, hollow, thin cylinder with a pressure difference between the outside and the inside,

and a superimposed axisymmetrical contact pressure acting on the inside. Elastic, plastic and thermal strains are considered.

The mechanical treatment of the fuel is extremely simple; only thermal expansion and creep strains are considered. The strain and temperature distribution in the fuel are axisymmetrical in the model. The outer, rigid zone is assumed to be totally cracked (only compressive stresses); the thermal expansion is therefore calculated as that of a rigid bar. The material in the plastic zone is allowed to expand freely and is assumed to be stress-free, except for hydrostatic pressure.

A rigid annulus, the bridge, forms the boundary between the rigid and the plastic fuel zones. The position of the bridge, together with the temperature distribution in the fuel, determines the thermal expansion of the cracked pellet. The creep deformation in the fuel changes the position of the bridge. This change in position depends on the creep strain at the bridging annulus, and the total crack opening angle (see fig. 3.1).

The stress at the bridge is

$$\sigma_b = P_{cp} \cdot R_{fs}/R_b \qquad (3.1)$$

where P_{cp} is the contact pressure, R_{fs} the fuel surface radius, and R_b the bridge radius. The UO_2 creep, ε, at the bridge is found from the bridge temperature and σ_b by the UO_2 creep equation. The area occupied by the material from R_b to $R_b + dR$, as a result of creep, is

$$A_{cr} = 2\pi\varepsilon P_b dR \; . \qquad (3.2)$$

The crack area between R_b and $R_b + dR$ may be approximated by

$$A_{crk} = \pi(dR)^2 \cdot w/2\pi \; . \qquad (3.3)$$

Equating these areas (eqs. 3.2 and 3.3) yields the creep of the bridge

$$dR = 4\pi\varepsilon R_b/w \; . \qquad (3.4)$$

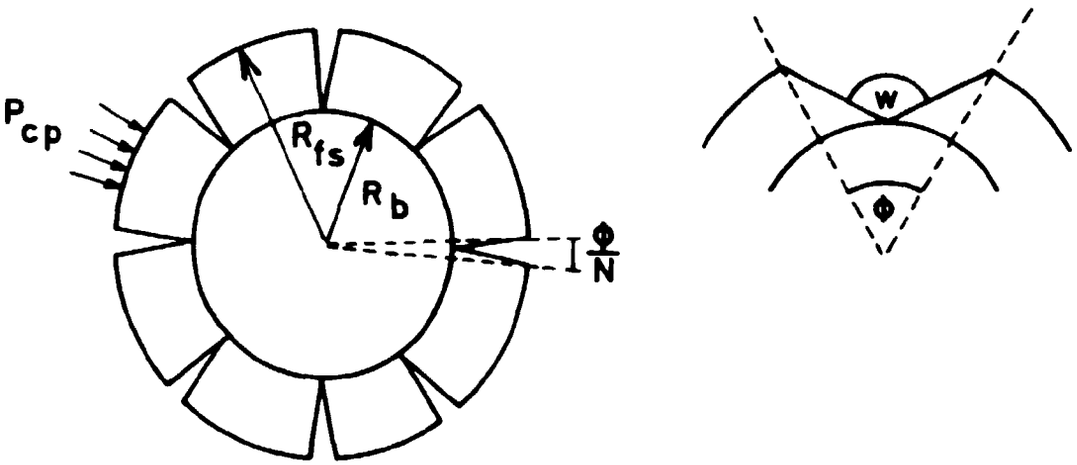

Fig. 3.1. Cracked pellet.

The connection between fuel and cladding is called the gap. The gap conductance is modelled according to Ross and Stoute[5] with modifications as proposed by Vitanza[6] taking into account the eccentricity.

3.2. The stationary solution for the fuel rod

The common stationary solution for the regions is found by simultaneous solution of the equations for the regions with specific boundary and initial conditions for the fuel rod. The boundary and initial conditions are, for example, outer cladding temperature, heat load, pressure (outer and inner), cold geometry, and material conditions.

The solution is found iteratively as shown schematically in fig. 3.2.

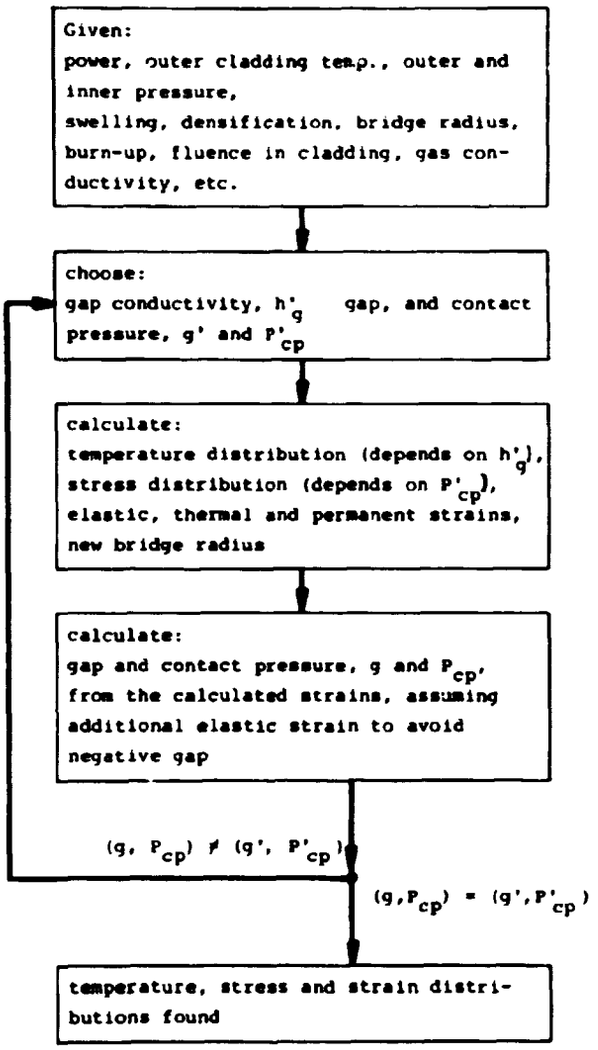

Fig. 3.2. Solution of the stationary equations.

3.3. The time-dependent quasi-stationary model

The stationary model as outlined in fig. 3.2 includes creep in fuel and cladding; however, the solution is found for a fixed time step, and the creep deformation is therefore treated as a time-independent plastic deformation.

The simulation of a realistic irradiation case requires that time-dependent boundary conditions be considered as well as changes in the materials with time.

During a period of constant heat load, the most important changes result from creep and those in the material itself, such as swelling, densification, and fission gas release.

The solution is obtained by an incremental theory; the temperature distribution from the last time-step is used in the evaluation of swelling and fission gas release during the time-step considered, but stress, strain and temperature distributions are found for the time-step as shown in fig. 3.3.

Power ramps are divided into "small" ramps. In each "small" ramp the bridge is moved a fraction of the pellet radius towards the centre and then allowed to creep back as far as the creep rate and the time allow. Hence the bridge position is fixed by a balance between ramp rate and creep rate at the bridging annulus.

During a fall in heat load the bridge position is assumed to be unchanged in the model. The power level, at which the thermal expansion again starts moving the bridge towards the centre, in a new ramp, decreases with burnup from a previous level. At this power level the thermal expansion again begins to move the bridge toward the centre, thereby opening the cracks.

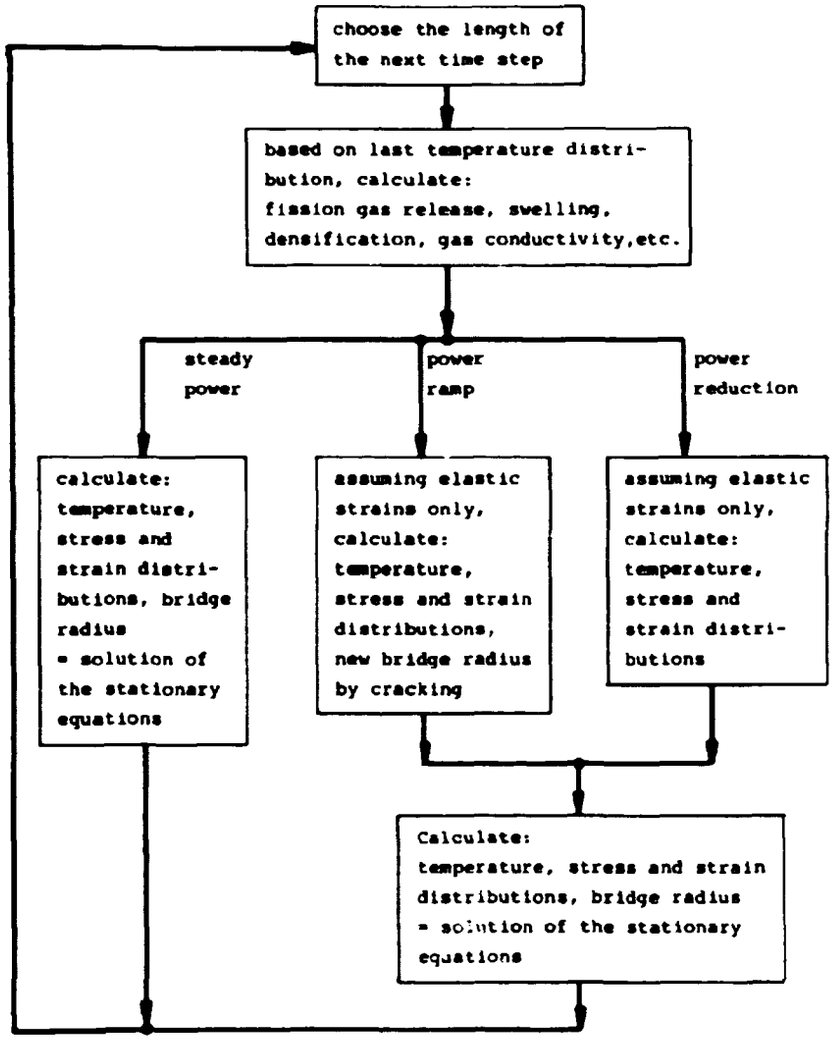

Fig. 3.3. The time-dependent, quasi-stationary model FFRS.

3.4. Verification of FFRS

The fuel model was verified in a number of irradiation experiments including the EPRI benchmark cases[7]. The result generally agreed well with the experimental results (for the EPRI benchmark cases, it proved to be as good as any of the compared codes). A few results are listed in table 3.1 together with the experimental values.

Further results and illustrations of the code performance are given in reference 4.

Table 3.1. Comparison between experimental PIE data and the values calculated by FFRS

Pin no.	EOL average strain		Max. temperature		Released fission gas	
	exp %	calc. %	exp. °C	calc. °C	exp. %	calc. %
M20-1B	-0.35	-0.29	1950	2100	40	35
Pa29-4	-	-0.25	1900	2260	47	61
M2-2C	-	-0.36	1850	2070	37	49
AG17-2	0	-0.16	-	1970	-	21
AG17-3	-0.15	-0.17	-	1960	3	22
HCD	0.2-0.3	0.16	1232*	1268*	(2.3)	22
X-260	0.28	0.21	2015	1970	-	-
X-264	0.36	0.16	2166	2140	-	-
ELP-9	-	-	2200	2230	23	19
PWR Rod	-0.59	-0.71	1650	1860	12.7	5

* at 4710 MWd/MTU and 400 W/cm

4. FUEL FAILURE CRITERIA

The failures observed in nuclear fuel pins today are normally characterized as pellet-cladding interaction, PCI failures. They are caused by high tensile stresses in the cladding during a power increase where the expansion of the fuel exceeds that of the cladding.

The strain observed for failed fuel is often below the out-of-reactor fracture strain for irradiated fuel cladding; therefore, the failure mechanism is generally described as stress-corrosion. This is supported by out-of-reactor experiments, where it is shown that the fracture stress for zircaloy tubes is reduced if the tubes are exposed to iodine vapor at temperatures above 220°C (refs. 8-17). For these stress corrosion failures the fracture surfaces do resemble those seen on failed fuel[8], and it has been demonstrated that the fission products released from hot irradiated fuel can reduce the fracture stress for zircaloy tubes [9,10].

These observations all indicate that the failure mechanism can be characterized as stress corrosion, and the experimenters propose iodine as a possible corrosive element. Unfortunately, no stress-controlled experiments have until now been performed with fission products present, neither out-of-reactor nor in-reactor. Therefore the influence of the in-reactor environment in a fuel tube cannot be described quantitatively.

An expression for the time-to-failure for stress corrosion, depending on the tube material and the fuel state, has been derived from the results of out-of-reactor stress corrosion experiments performed with unirradiated zircaloy exposed to iodine vapour.

Very recently, some results from out-of-reactor stress corrosion experiments performed on irradiated zircaloy tubes exposed to iodine vapour have been published[11]. These results differ considerably from those derived from experiments with unirradiated tubes. Corrections which would enable the results from both to be more closely correlated have been proposed.

As there do not exist, at the moment, any experiments which can quantify the influence of the in-reactor environment, the only calibration possible with respect to this environment is obtainable by means of ramp experiments. Here the stresses are calculated by a fuel performance code.

Additional failure criteria, which under special conditions could become important, are creep rupture, overstrain and fatigue.

4.1. Time-to-failure for stress corrosion

The time-to-failure for stress corrosion consists of the time to crack initiation plus the time to crack propagation; however, in this simplified formulation no distinction is made.

Assuming that the time-to-failure for stress corrosion, t_{FSC} can be approximated by a product of several independent functions,

each function expressing the dependence of a single or a few parameters, an expression is derived of the form

$$t_{FSC} = f_1 \text{ (environment)} \cdot x\ f_2 \text{ (stress, material condition)} \cdot x\ f_3 \text{ (temperature)}. \quad (4.1)$$

4.1.1. Influence of the environment

In the stress corrosion tests, the dominant environmental factor is the iodine concentration influenced by the presence of catalyzing components (air, iron, etc.). During in-reactor situations the environment is almost unknown, but at least two possibilities for the dependence on the fuel condition exists, namely:

1. The corrosive components are stable and are released with approximately the same rate as the noble gasses (Xe,Kr). In this case the corrosive concentration is proportional to the concentration of the released fission gas.
2. The corrosive environment exists mainly during transient release, caused by high thermal and chemical instabilities.

Experiments have been performed (for example see refs. 9 and 10) which demonstrate the influence of the fission products, but no experiments have yet tried to distinguish between the two mentioned possibilities.

Until further experiments are available the corrosive components are assumed to be proportional to the concentration of released fission gas. The dependence of the time to failure on the corrosive concentration is based on iodine stress corrosion experiments, as for example the experiments of Wood[12] and Elayaperumal and Bulenchandra[13]. The trend observed in these experiments is shown in fig. 4.1.

The figure shows three areas: In area I the specimens fails in approximately the same time as specimens without iodine and the fracture surfaces look like creep rupture fractures. In areas II and III brittle fractures are observed. No significant decrease in the time-to-failure with increased iodine concentration is observed in area III.

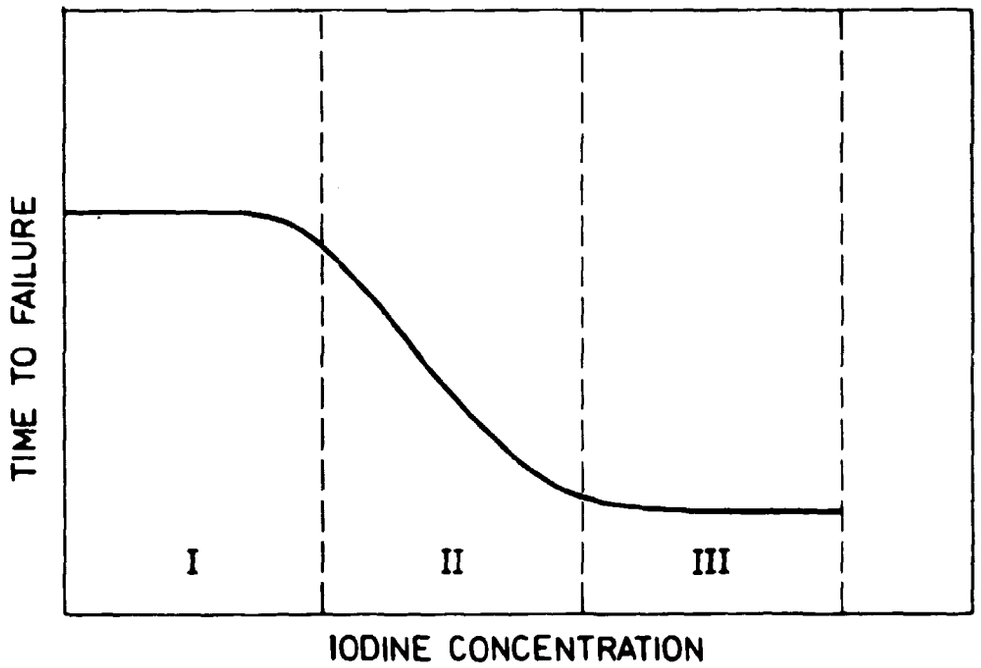

Fig. 4.1. Influence of the iodine concentration on the time-to-failure in stress corrosion experiments.

The expression used for f_1 is

$$f_1 \text{ (environment)} = f_1 \text{ (fission gas concentration)} = \frac{\text{const}}{\min(P_o, P)} \qquad (4.2)$$

where P_o is the fission gas pressure corresponding to the saturation level, and P is the partial pressure of fission gas in the fuel pin.

4.1.2. Influence of the temperature

The influence of the test temperature on the time-to-failure for iodine stress corrosion have been investigated by several authors. The data from Wood[12], Busby et al.[14] and Weinberg[15]

agree well with a temperature dependence where a 40°C increase in the temperature corresponds to one decade decrease in the time to failure, this is approximately valid between 220°C and 400°C. The lower temperature limit for stress corrosion in iodine vapour is around 220°C.

The expression used for f_3 is

$$f_3(\theta) = \text{const} \times 10^{\frac{220-\theta}{40}} \; ; \quad 220^{\circ}C \leq \theta \leq 400^{\circ}C \qquad (4.3)$$

where θ is the temperature in °C.

An expression of this form could be expected if the dominant process is a chemical reaction, as, for example, the crack initiation process.

4.1.3. Influence of the stress and the material condition

The time-to-failure in stress corrosion tests depends strongly on the materials used; different amounts of cold work and differences in the heat treatment have a strong influence. One way to characterize the materials is through the yield strength or the ultimate burst strength measured in a uni-axial or bi-axial test. If the time-to-failure is plotted versus the stress for different materials (otherwise equal conditions), the curves appear as shown in fig. 4.2.

It is possible to multiply the stress for each of the three materials in fig. 4.2 by individual factors, chosen so that the curves a, b, and c coincide. These factors are approximately proportional to the reciprocal of the ultimate burst strength, σ_u. For very hard materials, normalization with σ_u seems to lengthen the time-to-failure, and a limit value for the normalization stress is assumed.

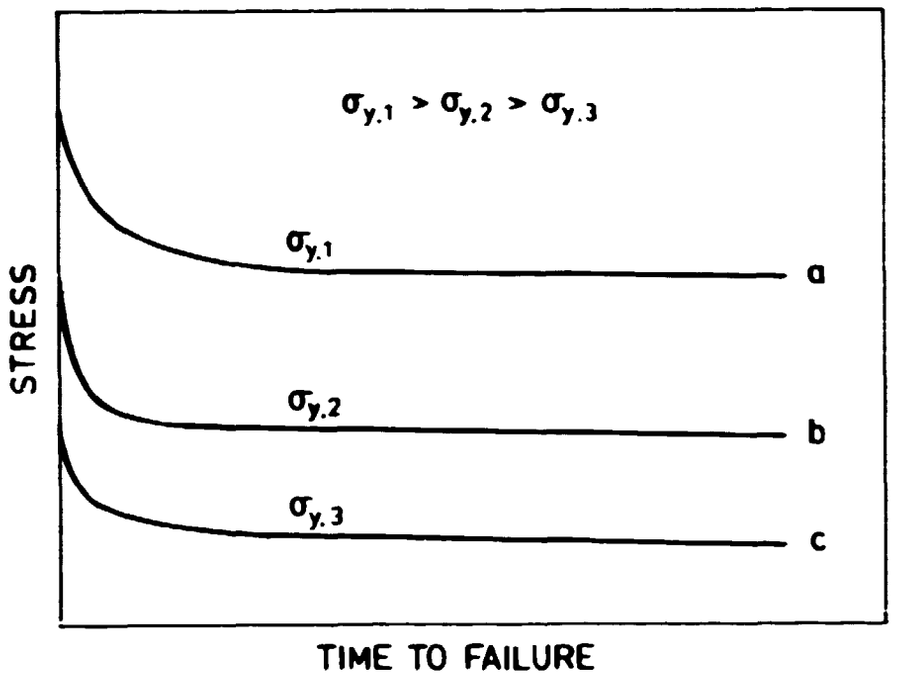

Fig. 4.2. Influence of the material condition on the time-to-failure versus stress.

f_2 can then be expressed as

$$f_2 \text{ (stress, material condition)} = f_2(\sigma_N) \qquad (4.4)$$

$$\sigma_N = \sigma/\sigma_u;\ \sigma_u = \min\ (\sigma_{u,burst},\ \sigma_{u,limit})$$

Because of the influence of a number of uncontrolled parameters such as the residual stresses, catalyzing components, and texture, a single investigation, that of Busby et al.[14], provided the data for estimating $f_2(\sigma_N)$. The data are shown in fig. 4.3; they are for both annealed and stress-relieved tubes tested at 360°C and 400°C. The iodine concentration has been varied in the test, but no significant influence was observed.

In fig. 4.4 the data are shown plotted against the normalized stress; the different test temperatures have different scales on the abscissa, corresponding to the expected differences in

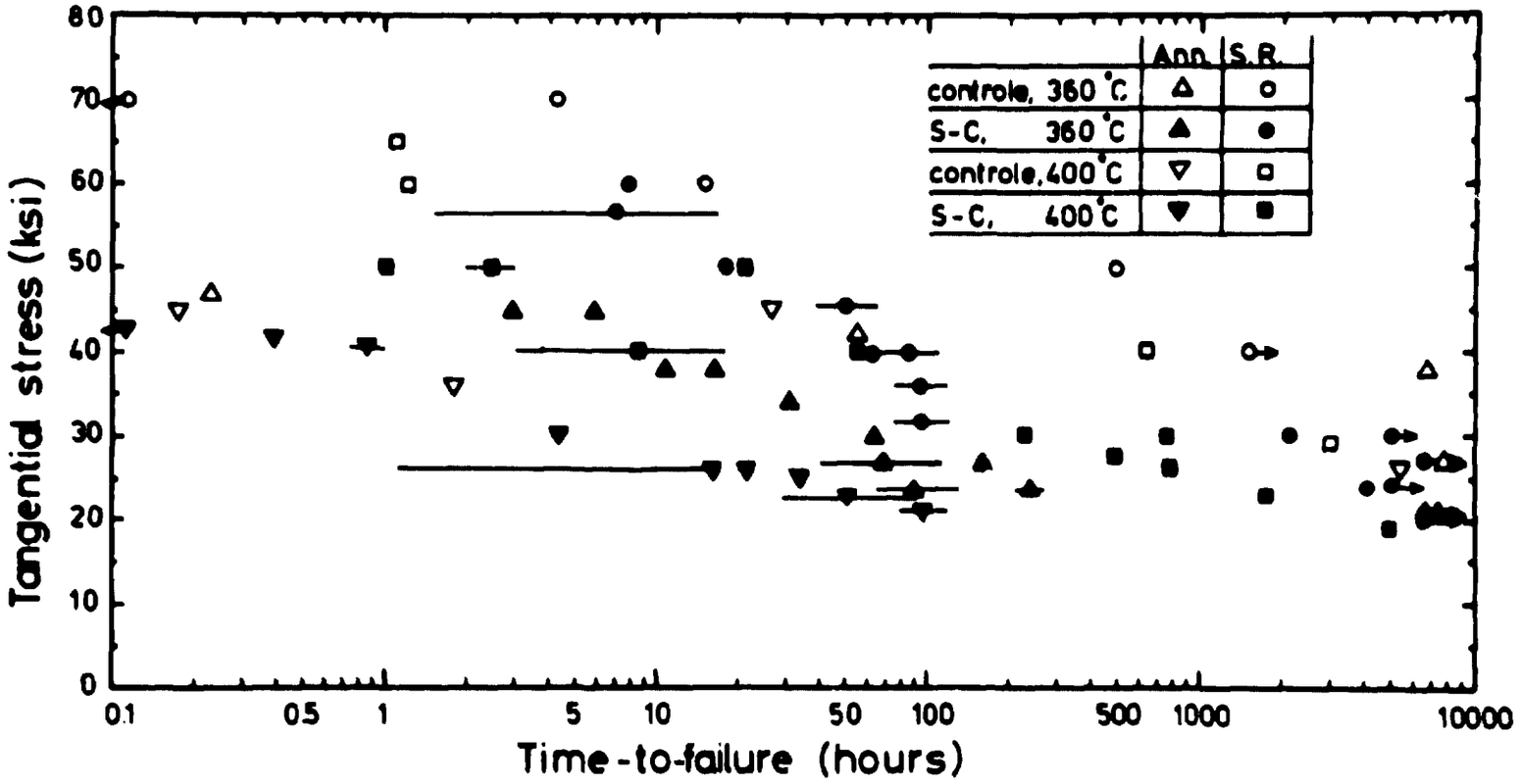

Fig. 4.3. Variation of time-to-failure with the hoop stress for two different material conditions at 360°C and 400°C. The data are from Busby et al.[14].
S.R. = stress-relived tubes, Ann = annealed tube.

time-to-failure (according to f_3). On the figure f_2 (σ_N) is shown. In FRP a piecewise linear (in th. semilogarithmic figure) approximation to f_2 (σ_N) is used.

Based on the data from refs. 14-17 a value of approximately 550 MP is found for $\sigma_{u,limit}$ at 360°C.

4.1.4. Irradiated cladding

Very recently, several experiments performed on irradiated cladding tubes have been published by Roberts et al.[11]. The experiments are performed out-of-reactor with iodine as the corrosive component.

These experiments show that there are large differences between the hard irradiated fuel tubes and the hard unirradiated tubes with respect to stress corrosion.

I fig. 4.5 the time-to-failure versus the normalized stress for the irradiated fuel tubes is plotted; the normalization stress is 550 MP as for hard unirradiated tubes. In the figure $f_2(\sigma_N)$ is also shown. The stress necessary for stress corrosion is much less for the irradiated cladding. If a normalization stress around 400 MP were used and the time-to-failure were multiplied by a factor of 100, the experimental points obtained for irradiatec cladding would fall close to f_2.

However, it should be noticed that these few experimental points verify neither the stress dependency as expressed by f_2 and the normalization stress, the temperature dependency, nor the dependency on the concentration of fission gases.

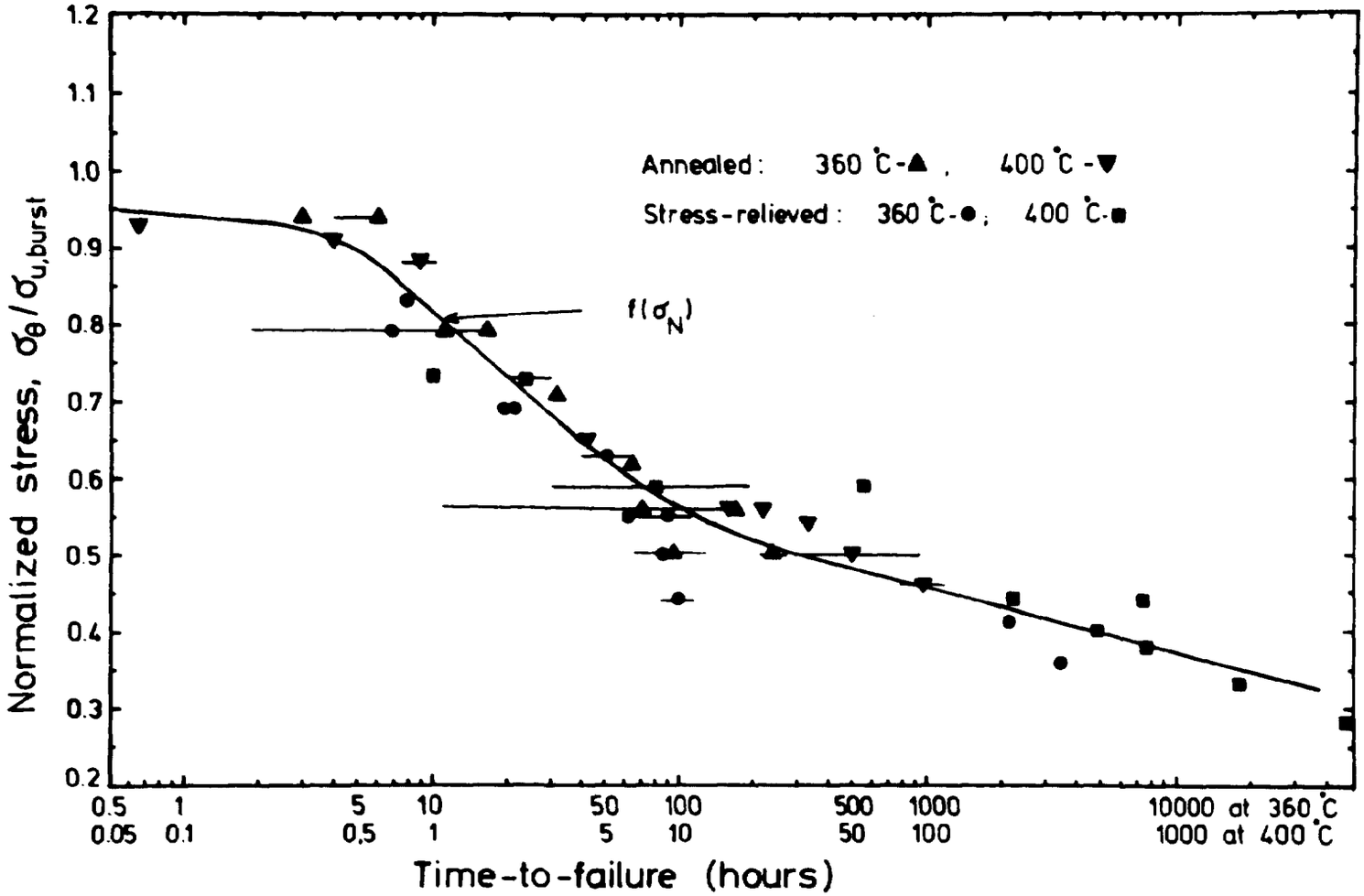

Fig. 4.4. Dependence of time-to-failure with the normalized stress for two different material conditions. The two different experimental temperatures are compensated by the different time scales. The data are from Busby et al.[14].

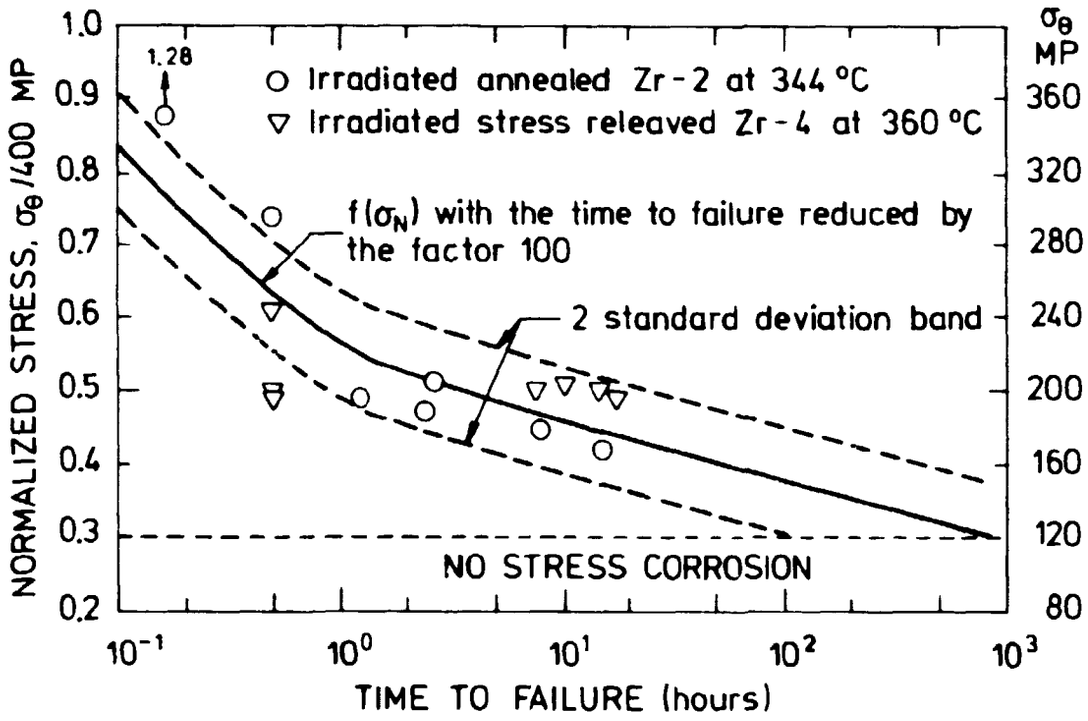

Fig. 4.5. Time-to-failure for irradiated zircaloy.

4.2. Failure criteria under varying conditions

In a fuel rod the parameters important for stress corrosion are continuously changing. In order to utilize the data from stress corrosion experiments for the prediction of fuel failures, a cumulative damage process is assumed; it is furthermore assumed that the effect of two periods with different conditions is the same regardless of which period occurs first.

The extent of damage, ΔSCD_i, in a time inverval, Δt_i, with constant conditions, is defined as

$$\Delta SCD_i = \frac{\Delta t_i}{t_{FSC,i}} \qquad (4.5)$$

where $t_{FSC,i}$ is the time-to-failure according to 4.1 for the conditions given during the time period.

The damage following a number of time periods (1-n) is

$$SCD(t_n) = \sum_{i=1}^{n} \Delta SCD_i = \sum_{i=1}^{n} \frac{\Delta t_i}{t_{FSC,i}} . \qquad (4.6)$$

If the process is continuous this becomes

$$SCD(t_n) = \int_{t_o}^{t_n} \frac{dt}{t_{FSC}(t)} \qquad (4.7)$$

For stress corrosion the probability of failure at time t_n is then

$$P(\text{failure}) = P(SCD(t_n) > 1) \qquad (4.8)$$

The uncertainty of the time-to-failure under well-controlled conditions can be estimated from the experiments, where all parameters included in 4.1, with f_2 given by 4.4, are controlled. This uncertainty can be accounted for by replacing the failure criterion in 4.8 with a formulation such as D > R, where R, the normalized resistance, is a stochastic variable, which includes the above mentioned uncertainty.

5. MATERIAL AND DESIGN DATA

In the following a short summary is given of the basis for the data which are used in the reliability calculations with FRP. A more comprehensive treatment is found in ref. 18.

5.1. Design data

The design data, as well as their probability density functions, should be based on information available for the specific fuel treated. A few rules of thumb which are helpful in the estimation of the probability density functions for design data are:

The design parameters are assumed normally distributed.

The standard deviation can be estimated from the specified tolerances. A tolerance band for 100% inspection (cladding diameter, cladding thickness, gap size etc.) is associated with a 6 standard deviation band. A tolerance band for sample inspection (density, yield strength etc.) is associated with a 4 standard deviation band.

The value specified in the design specifications is used as the mean value.

5.2. Material data

The material data as well as estimates of the probability density functions are all described in ref. 18. If tests, performed on the same fuel as the fuel treated, are available for any material property, they should be utilized for reestimation of the probability density function for this material property.

The uncertainty of a material property originates from several sources: experimental uncertainty, insufficient experimental data, lack of knowledge of the physical background, and uncontrolled (not included in the equations) differences in material composition and structure.

Very often the equation for a specific material property is a fitted function, where the constants themselves are correlated. As the available data points seldom are sufficient to determine the distribution of all the constants and the correlation between them, an expression of the form $\gamma = g(\text{time, temperature etc.}) \cdot F$, where γ is the material equation used in deterministic fuel modeling and F is a stochastic variable including the total uncertainty for this material property. The mean value (mean function) for γ is called g. F is determined by comparing experimental values for γ with the values calculated by g. If g contains constants (or terms) which can be considered independent (by physical arguments) they are treated separately.

For most of the material properties the expressions from two recent investigations of material properties for zircaloy and UO_2, MATPRO[19] and EPRI[7] together with additional equations published in the literature were considered. In MATPRO quite comprehensive comparisons with experimental data are often included; these are then used to estimate the distributions of the material properties. Where necessary, further experimental data are included.

Example: Zircaloy creep is described by an equation proposed by Gittus et al.[20]. The uncertainty in the creep is associated with a factor F = experimental/calculated creep. The distribution of F has been estimated from 65 experimental in-reactor creep measurements. It was found that F is log-normally distributed with the mean value 1.2 (median 1.0) and a standard deviation of 0.5.

It should be noted that the distributions for the material data are based on literature-derived data from various sources; they include uncertainties attributed to missing experimental information. Consequently, the distributions are not typical of a single case; reduction of the uncertainty, therefore, would require experimental data for each fuel batch.

For a deterministic calculation in which prediction of the results obtained in an experiment are sought, the most probable value, i.e., the mode value, should be used for each of the material parameters.

6. NUMERICAL RESULTS FOR THE STATE VARIABLES

When utilizing a statistical program like FRP the choice of numerical method is a compromise between the desired accuracy and the computational effort to be spent. The most reliable method available in FRP is Monte Carlo simulation with a very large number of trials; however, each trial requires detailed

simulation of a fuel pin during its irradiation history, and the computational effort is therefore extremely high. Depending on the kind of information desired, alternative methods requiring less computations are available.

The desired information can roughly be characterized as data regarding (a) the central parts of the pdf's for the state variables, and (b) the tails of the pdf's for some of the state variables. For the evaluation of irradiation experiments, where only a single or a few pins are considered, the information desired for the state variables is an estimate of the mean value or the mode value together with the width of some confidence intervals. This information is connected with the central part of the pdf's. If the failure probability of commercial fuel, where a large number of fuel pins are considered, is desired, it is often necessary to estimate the tails of state variables included in the failure criteria.

Information regarding the central part of the pdf's can be obtained by Monte Carlo simulations with a relatively small number of trials, or, if the pdf's are well behaved, by a low order Taylor approximation. In both cases the computational effort can be reasonably small.

An estimate of the tails of a given distribution is more difficult, but if the pdf for the considered state variable is well behaved, it is possible to extrapolate the tails from the central part by assuming a known probability density function. The same procedure applies for the Taylor approximation where the probability density function can be derived from the calculated moments.

If the reliability is expressed by a reliability index, only the mean value and the standard deviation need be estimated, even when the failure probability is desired.

A priori knowledge about both the pdf's for the state variables and the truncation errors when applying the Taylor approximation is therefore important for efficient utilization of the methods.

6.1. Distribution of the state variables

The distribution of the state variables depends on the pdf's for the material and design data as well as on the transfer function (which depends on the power history and the simulation model). A general description of the pdf's for the state variables can therefore not be given; they can, however, be illustrated by a typical example, such as is described in Appendix A.

With the transfer function (power history and simulation model) and the nominal design and material data as specified in Appendix A, approximations to the probability density functions for the state variables have been calculated by Monte Carlo simulations.

For most of the state variables the probability density functions are well behaved; examples of these state variables are the fractional release of fission gas at end-of-life and the end-of-life permanent strain of the cladding tube. Frequency polygons based on 500 Monte Carlo trials are shown for these two variables in figures 6.1 and 6.2.

The fractional release of fission gas seems to follow a lognormal or an extreme value (largest value) distribution. In figure 6.3 the cumulative distribution function, CDF, for the fractional release is shown on lognormal probability paper (a lognormal CDF fits a straight line in the plot). Though there are some diviations from a straight line, the lognormal distribution function seems to be a reasonable description of this variable. The end-of-life strain appears similar, except that this distribution is skewed to the left, and is bounded neither to the left nor right. An extreme-value distribution (smallest element) seems to model the distribution for this variable reasonably well.

The distribution for a few of the state variables is not well behaved. The cause of this must be sought in the transfer function, which for these variables is very unlinear. These

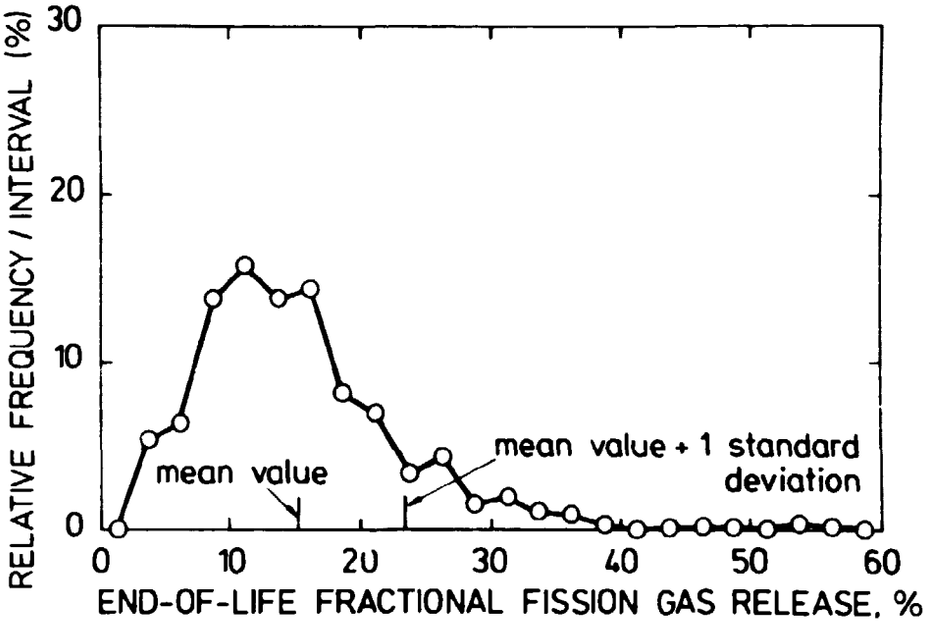

Fig. 6.1. Frequency polygon for the end-of-life fractional fission gas release, based on 500 Monte Carlo trials.

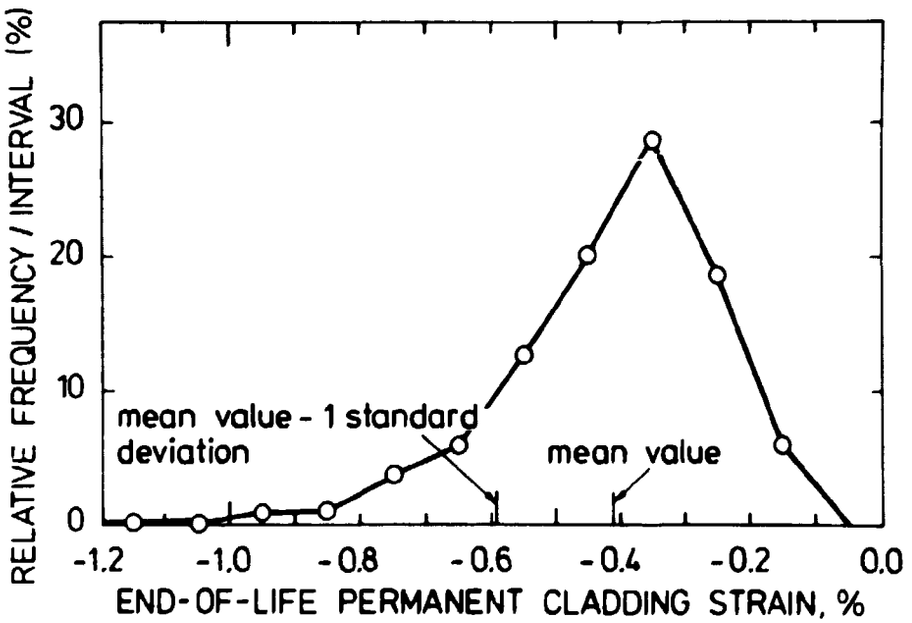

Fig. 6.2. Frequency polygon for the end-of-life permanent cladding strain based on 500 Monte Carlo trials.

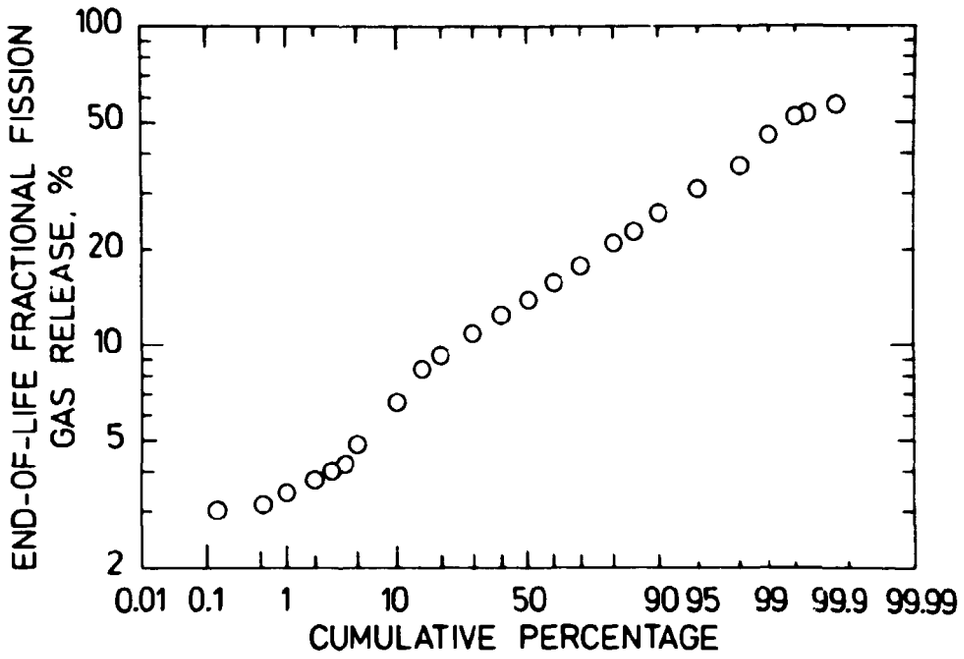

Fig. 6.3. Lognormal probability plot for the end-of-life fractional fission gas release.

state variables all depend on the cladding tangential stress, which is responsible for the high unlinearity in the transfer function for these variables, as is the difference between situations with and without contact between fuel and cladding. A transfer function of this type is illustrated in figure 6.4. The first almost horizontal part corresponds for the peak stress to a situation with no contact between fuel and cladding, in this area the peak stress is insensitive to the considered design or material variable. The second area corresponds to irradiations where the deformations of the cladding are elastic. In area III the interaction is strong enough to cause plastic deformations of the cladding.

A frequency polygon based on 500 Monte Carlo trials is shown in figure 6.5 for the maximum tangential stress in the cladding. It illustrates the behaviour of the state variables depending on the cladding stress.

One of the state variables for which estimation of the tail is very important, is the stress corrosion damage index, D. The calculation of this index is based on the tangential stress in

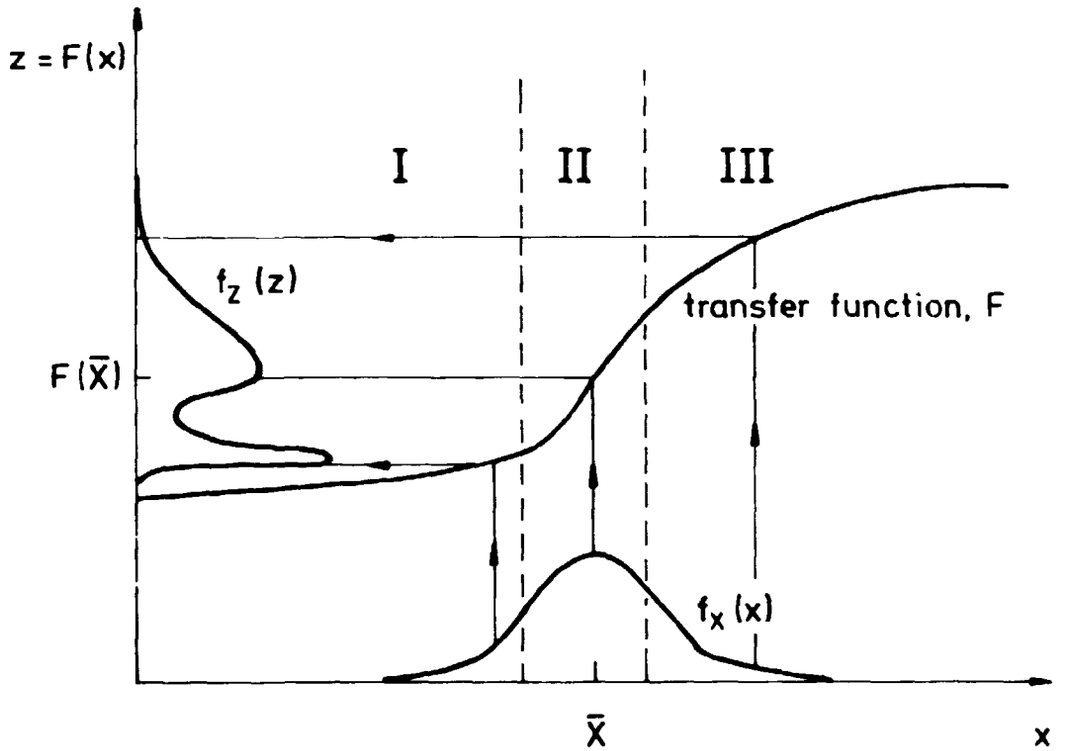

Fig. 6.4. Example on the influence of an nonlinear transfer function.

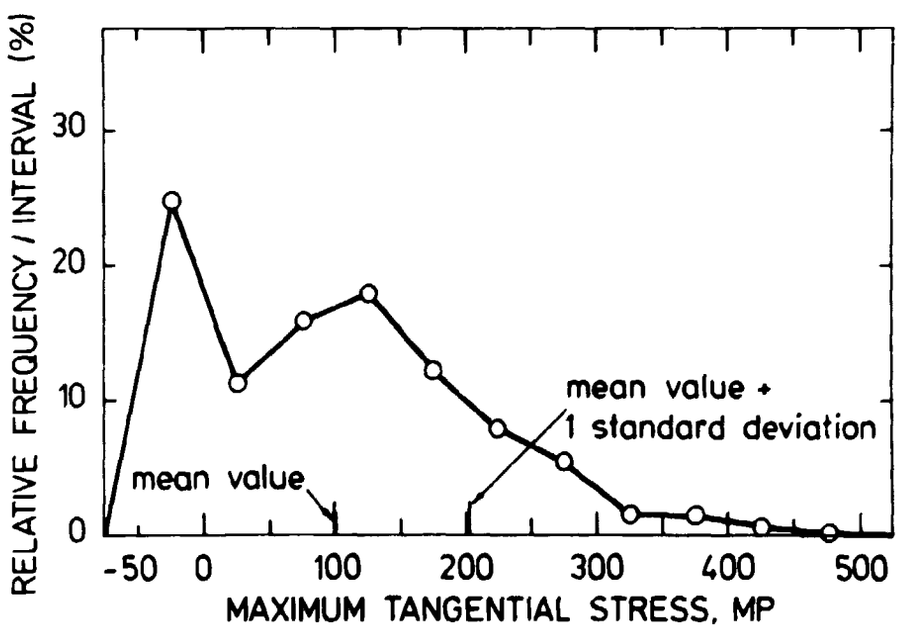

Fig. 6.5. Frequency polygon for the maximum tangential cladding stress, based on 500 Monte Carlo trials.

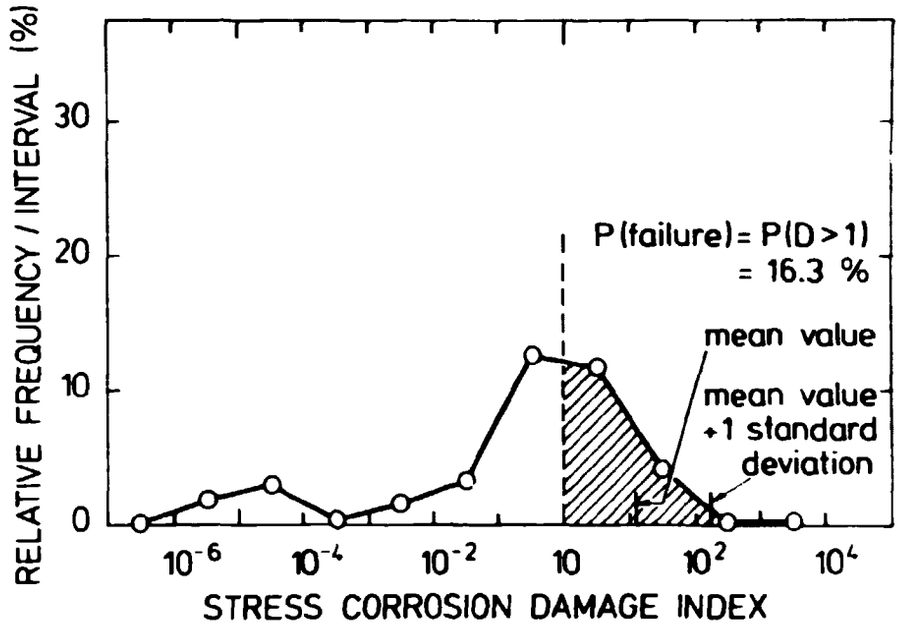

Fig. 6.6. Frequency polygon for the stress corrosion damage index, based on 500 Monte Carlo trials.

the cladding and the time to failure correlation, equation 4.6. The distribution of the damage index is illustrated in figure 6.6, where a frequency polygon based on 500 Monte Carlo trials is shown. In approximately 60 per cent of the trials, the stress never reaches the lower limit for stress corrosion, and the damage index is zero. This pdf is difficult to extrapolate from calculations with a small number of trials, and the moments alone give almost no information as their values are dominated by a few trials. If, for example, the highest value for the damage index is excluded from the 500 Monte Carlo trials used in figure 6.6, the mean value would be 2 instead of 12.

In attempting to avoid this distribution in the calculation of the failure probability, the stress corrosion damage index is transformed to a stress corrosion damage stress, S_D, defined as the stress for which the time to failure calculated by equation 4.6 under specified conditions (for example: irradiated cladding, 360°C, and saturation of the fission gas pressure) is equal to 1/D. It is possible to define a stress different from zero,

also when the damage index is zero. Another advantage of using this damage stress for the calculation of the failure probability is,that the resistance is defined in terms of the failure stress at 360°C with the time to failure equal to 1 hour. Therefore the resistance is uncorrelated with the stress corrosion damage stress, and the distribution of the resistance can be estimated from stress corrosion experiments. In this case the failure probability can be calculated by equation 2.2.

A frequency polygon is shown in figure 6.7 for the stress corrosion damage stress. The pdf resembles that of the maximum stress, but the tail does not seem to follow any simple probability distribution function. The moments for this variable are not sensitive to the small number of trials as are the moments for the damage index.

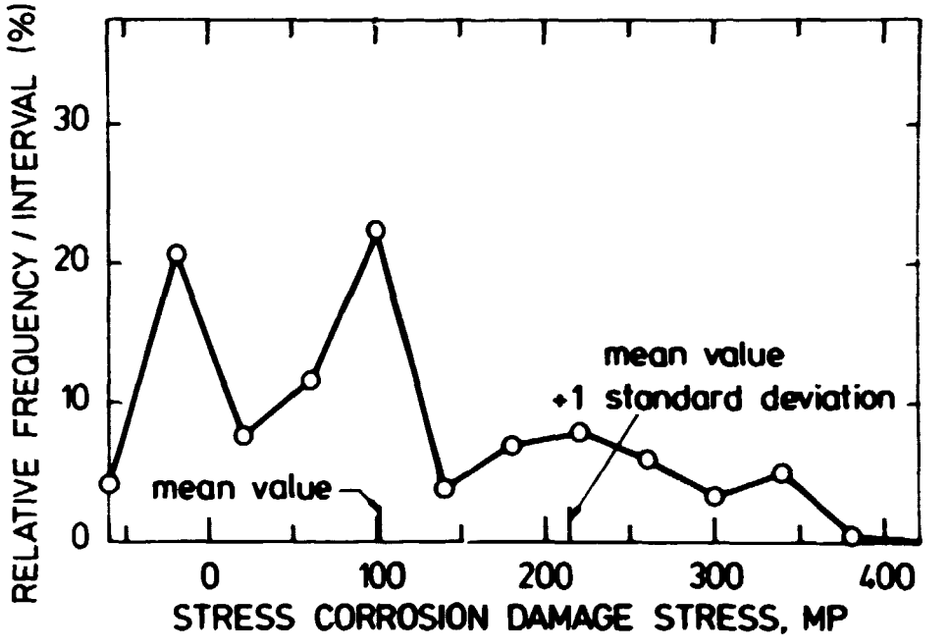

Fig. 6.7. Frequency polygon for the stress corrosion damage stress, based on 500 Monte Carlo trials.

For most design and material data the distributions are based on rather small samples; the tails of these distributions are, therefore, only an extrapolation of the central values. The significance of the tails is investigated by performing Monte Carlo simulations with the pdf's of all design and material data truncated at the α and $100-\alpha$ per cent fractile.

The simulations were performed with α = 5, 1 and 0.14 per cent, corresponding to a normal pdf truncated at $\pm$ 1.6, $\pm$ 2.3, and $\pm$ 3.0 standard deviations respectively.

Tables 6.1 and 6.2 show the fractions exceeding the 5, 1, and 0.14 percentiles in the untruncated distributions for the maximum stress and stress corrosion damage stress respectively. The same random sequence with 500 trials is used for the four simulations.

The influence of the truncations is moderate; the pdf's for the state variables are not truncated at the same fractiles as the material and design data, the tails are only lowered.

Table 6.1. Influence on the peak stress of truncating the design and material data at the α and $100-\alpha$ per cent fractiles.

α %	fraction exceeding 246 MP %	fraction exceeding 281 MP %	fraction exceeding 378 MP %
0, untruncated variables	10.0	5.0	1.0
5.0	6.0	3.6	0
1.0	9.6	5.4	0.8
0.14	10.0	5.0	1.0

Table 6.2. Influence on the stress corrosion damage stress of truncating the design and material data at the α and 100-α per cent fractiles

α %	fraction exceeding 266 MP %	fraction exceeding 322 MP %	fraction exceeding 350 MP %
0, untruncated variables	10.0	5.0	1.0
5.0	9.0	2.0	0.0
1.0	10.4	4.6	0.6
0.14	10.4	5.2	1.0

6.2. Accuracy of the Taylor approximation

As shown in section 6.1, the probability density functions for most of the state variables are well behaved. Approximations to the lowest moments would satisfactorily characterize these state variables for most applications. We can evaluate these approximations either by Monte Carlo simulations or by a Taylor expansion.

The accuracy of the Taylor expansion depends on both the distribution of the design and material data and the transfer function; this dependence was investigated numerically using data specified in Appendix A. In order to investigate the asymptotic behaviour of the Taylor approximation, when the variance of all the considered design and material data approaches zero, the standard deviation for all design and material data are multiplied by a factor, a; a = 1 corresponds to the nominal distributions as specified in Appendix A. The reference values (true values) are obtained by Monte Carlo simulations with 500 trials each.

Calculation of the Taylor approximation requires knowledge of the partial derivatives of the state variables with respect to all stochastic variables in the design and material data; these derivatives are evaluated numerically. The partial derivative of the state variable, $Z_i = F_i(\underline{X})$, with respect to the stochastic variable, X_j, is calculated from a polynomial approxi-

mation to a number of values $Z_{i,k} = F_{i,k}(\underline{\bar{X}})_{j,k}$, where $\underline{\bar{X}}_{j,k}$ specifies that all design and material data are at their mean values, except for X_j which is $\bar{X}_j+\Delta_k$. The change, Δ_k, can, for example, be plus or minus a fraction of the mean value. In this investigation five values for $Z_{i,k}$ were used, they are $\Delta_k = \bar{X}_j$, $1.1\cdot\bar{X}_j$, $1.2\cdot\bar{X}_j$, $0.9\cdot\bar{X}_j$ and $0.8\cdot\bar{X}_j$. The values $Z_{i,k}$ are calculated by the simulation model FFRS. This can cause some problems, since FFRS includes discontinuous submodels and the numerical accuracy is relatively low. These inaccuracies can overshadow the influence of some of the design and material data, if the values of Δ_k are too close to the mean value. The problems are easily detected by the dependency of the partial derivatives on Δ_k. For this example the influence was found to be small except for the stress corrosion damage stress, where the second order partial derivatives were very difficult to calculate accurately.

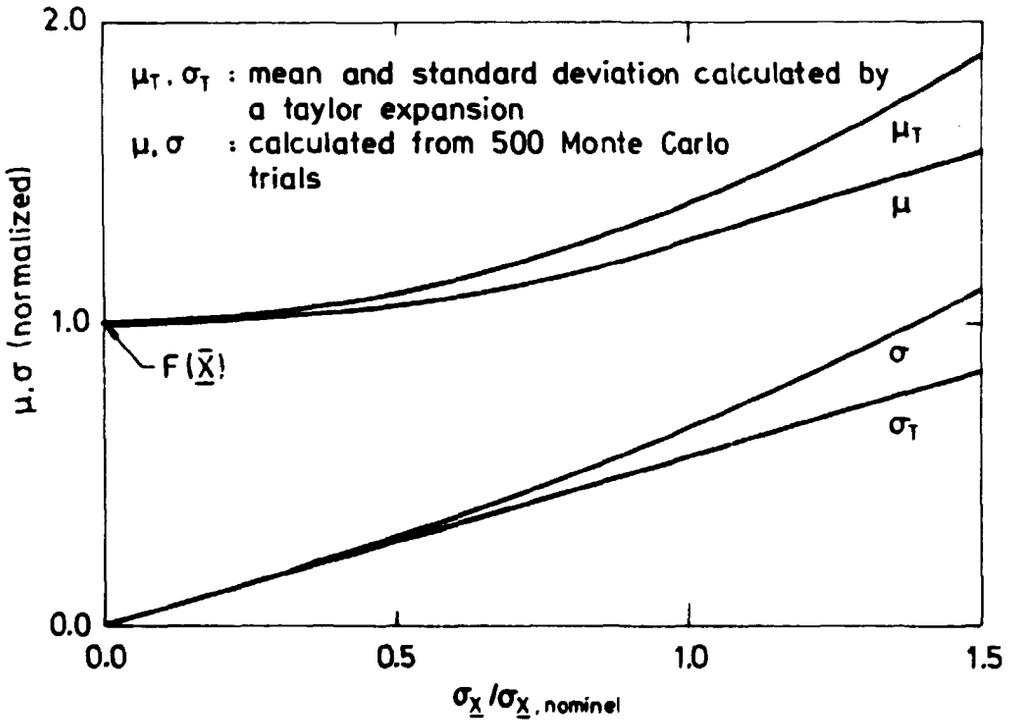

Fig. 6.8. Truncation error of the Taylor approximation as a function of the variation of the material and design data, shoen for the end-of-life fractional fission gas release.

The calculated mean values and standard deviations are shown in figures 6.8 and 6.9 for the fractional fission gas release and the end-of-life strain. For these state variables, the accuracy of the Taylor approximation is very good, even though the coefficient of variation is as high as 50%.

A comparison between the Monte Carlo simulation and the Taylor approximation is shown in figures 6.10 and 6.11 for the maximum stress and the stress corrosion damage stress. Despite the pronounced nonlinearity of the transfer function and the large variance for the damage stress, the Taylor approximation is reasonably accurate for the maximum stress. The Taylor approximation to the stress corrosion damage stress diverges considerably from the Monte Carlo simulation for a as low as 0.1. The low order Taylor approximation can therefore not be used for this variable in the nominal case, a = 1.

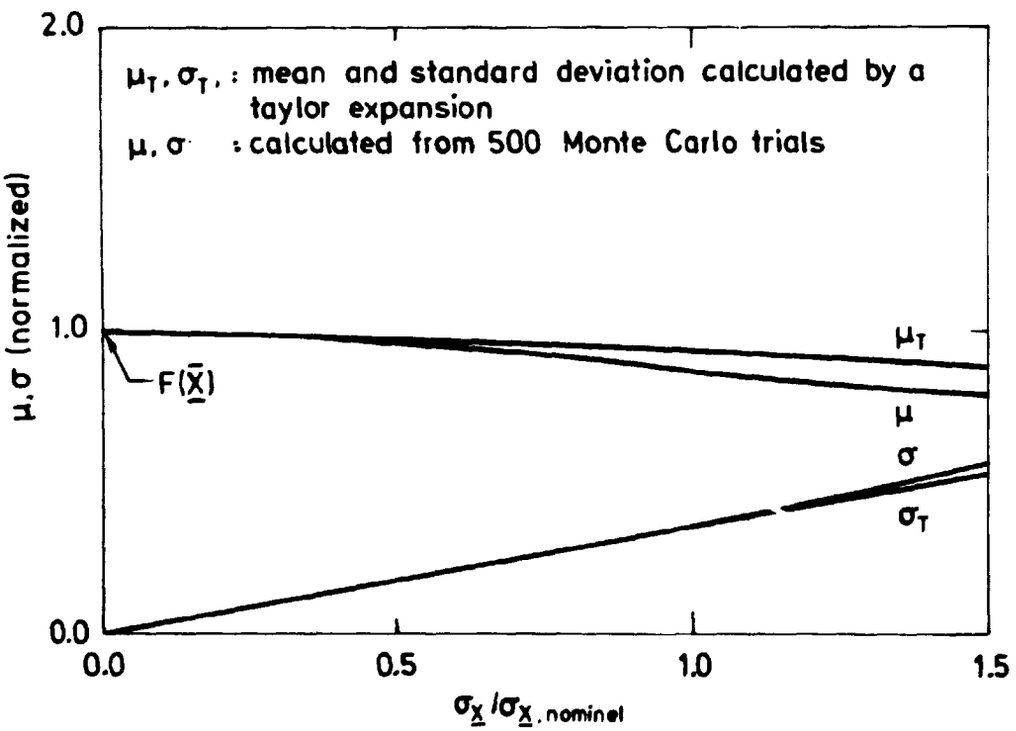

Fig. 6.9. Truncation error of the Taylor approximation as a function of the variation of the material and design data, shown for the end-of-life permanent cladding strain.

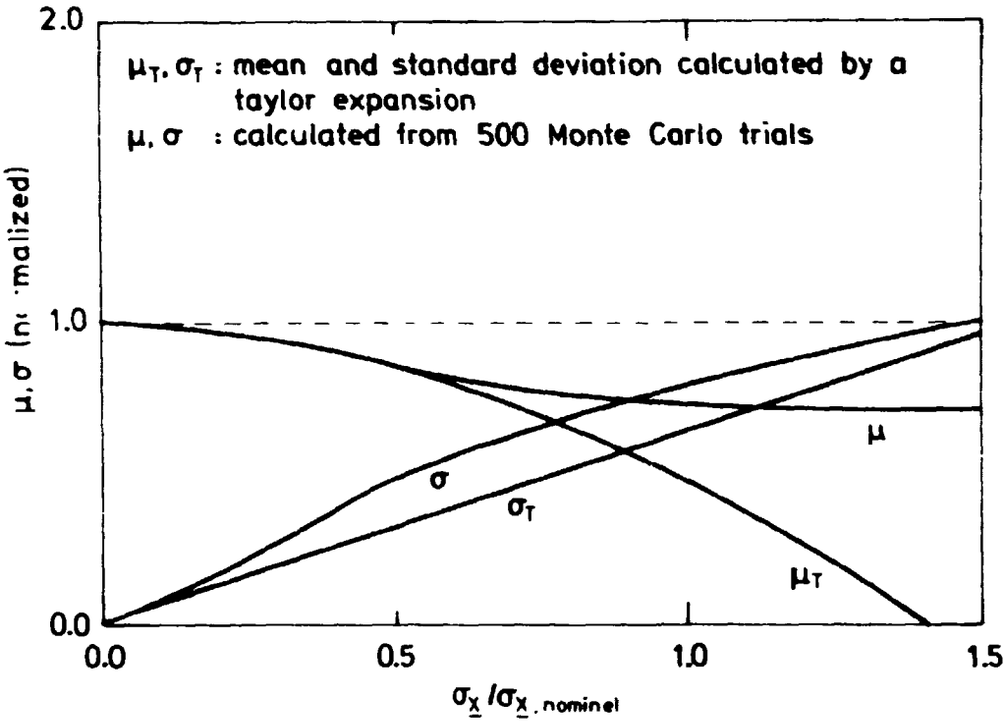

Fig. 6.10. Truncation error of the Taylor approximation as a function of the variation of the material and design data, shown for the maximum stress.

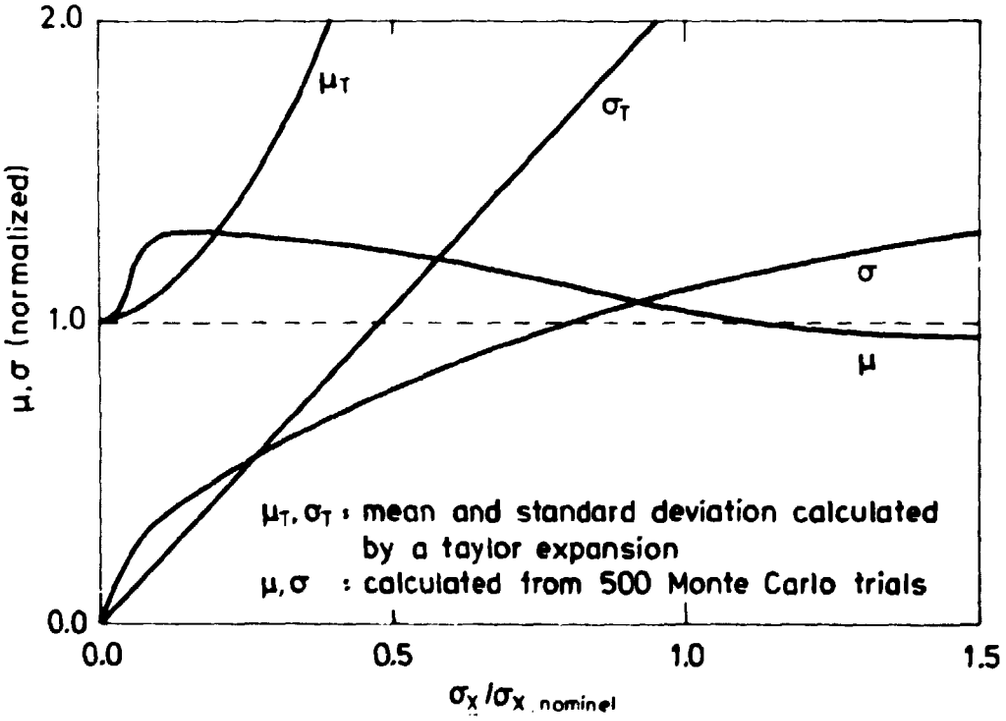

Fig. 6.11. Truncation error of the Taylor approximation as a function of the variation of the material and design data, shown for the stress corrosion damage stress.

6.3. Calculations with reduced computer costs

The computer costs for the Monte Carlo simulations and the Taylor approximations in sections 6.1 and 6.2 are moderate, nevertheless in some applications it is essential to obtain information on fuel performance at very low computer cost. These applications are, for example: (a) core performance calculations, where a large number of fuel pins throughout the reactor core are evaluated consecutively, or (b) experiments with pin bundles. It can also be beneficial, in general, to perform preliminary calculations which give immediate results.

In the Monte Carlo simulations the computational effort is proportional to the number of trials and is therefore easy to reduce. For the Taylor approximation the number of deterministic calculations with FFRS used for the estimation of each partial derivative can be reduced. As the contribution to the mean and the variance from each of the material and design data is calculated independently, the calculational effort is proportional to the number of stochastic variables in the material and design data.

It is not possible, in general, to define the minimal necessary number of Monte Carlo computations required or the minimal number of calculations with FFRS needed for the Taylor approximation; but the accuracy gained in using different approximations is illustrated by calculations on the example described in Appendix A.

The results for four of the state variables are shown in table 6.3. For the Monte Carlo simulations the fraction exceeding the stress corrosion damage stress of 350 MP is also shown. For the simulations with less than 500 trials this figure is obtained by extrapolation of the right tail assuming a normal pdf.

The relative computer costs are shown in table 6.3,given as the number of deterministic fuel simulations with FFRS. The calculation times for typical simulations with FFRS are found in reference 4.

The Monte Carlo simulations are characterized by the number of trials and the Taylor approximations are characterized by the number of points used as well as the order of the polynomial approximation required in estimating the partial derivatives.

Table 6.3. Accuracy and computer costs for different approximations

Method	Computer costs	Released fission gas,% **	EOL permanent strain,%	Max. stress,MP	S-C damage stress, MP	Fraction of the S-C damage stress exceeding 350MP,%
MC, 1000*	1000	(15.5, 9.1)	(-0.42, 0.17)	(98, 107)	(103, 113)	1.1
MC, 500	500	(15.4, 8.1)	(-0.41, 0.17)	(98, 106)	(103, 112)	1.0
MC, 150	150	(15.9, 8.4)	(-0.39, 0.16)	(100, 109)	(102, 113)	1.0
MC, 50	50	(14.9, 7.6)	(-0.38, 0.15)	(103, 110)	(104, 110)	2.0
MC, 10	10	(15.2, 4.6)	(-0.33, 0.08)	(73, 89)	(65, 86)	3.0
TA, 5, 2*	173	(16.8, 6.8)	(-0.44, 0.17)	(65, 86)	(785, 208)	-
TA, 5, 1	173	(12.0, 6.8)	(-0.47, 0.17)	(135, 86)	(100, 208)	-
TA, 3, 2	87	(16.6, 6.5)	(-0.43, 0.17)	(87, 83)	(1050, 186)	-
TA, 3, 1	87	(12.0, 6.5)	(-0.47, 0.17)	(135, 83)	(100, 186)	-
TA, 2, 1	43	(12.0, 6.3)	(-0.47, 0.16)	(135, 94)	(100, 205)	-
F($\bar{X}$)	1	(12.0, -)	(-0.47, -)	(135, -)	(100, -)	-
F(mode ($\bar{X}$))	1	(12.1, -)	(-0.35, -)	(108, -)	(108, -)	-

* MC, α = Monte Carlo simulation with α trials

TA, α, β = Taylor approximation utilizing α points and a polynomial of order β for the estimation of the partial derivatives.

** (μ, σ) = (mean, standard deviation)

7. CALCULATIONS PERFORMED WITH FRP

The computer code FRP has been utilized for the analysis of a number of problems. Examples on the analysis of irradiation experiments are presented in references 2 and 21. A comparison between two typical BWR designs, as well as the analysis of a minor accident - a control rod withdrawal at full power - are presented in reference 21. The examples from reference 21 are included as Appendix B.

As an illustrative example, the failure probabilities for two standard BWR designs have been evaluated for a given reference power history. In addition, the influence of changes in the power history and the influence of the uncertainty on the material and design parameters are illustrated.

7.1. Failure probability for the two BWR designs

The two fuel pin designs are chosen as a typical 7 x 7 BWR fuel pin and a typical 8 x 8 BWR fuel pin. The design data are shown in table 7.1, together with the distribution of the design parameters. The distributions are based on the typical tolerances given in ref. 18.

A few data for the reference power history are given in table 7.2.

Figure 7.1 shows the calculated failure probability as a function of the ramp time (the time to reach 25% overpower). The probability for the average strain to exceed the uniform limit (0.21%) is also shown; only instant plastic deformations and primary creep are considered.

The failure probability as a function of the overpower in the ramp is shown in fig. 7.2. The ramp time is 1 hour.

Table 7.1. Design data for the fuel pins

Specification	BWR 8 x 8	BWR 7 x 7
Inner cladding diameter (mm)	(10.8, 0.015)*	(12.42, 0.017)
Cladding thickness (mm)	(0.864, 0.022)	(0.94, 0.024)
Diametral gap (mm)	(0.228, 0.023)	(0.30, 0.03)
Density (% of theoretical)	(94.4, 0.66)	(94.4, 0.66)
Plenum volume	(37, 7.4)	(37, 7.4)
Fill gas pressure (atm)	(1, 0.2)	(1, 0.2)
Cladding yield strength, 300°C (MP)	(300, 15)	(300, 15)
Fuel grain size (μm)	(25, 5)	(25, 5)
Cladding surface roughness (μm)	(130, 26)	(130, 26)
Fuel surface roughness (μm)	(90, 18)	(90, 18)
Densification at 0.1% FIMA (%)	(0.16, 0.06)	(0.16, 0.06)
Densification at 1% FIMA (%)	(1.1, 0.4)	(1.1, 0.4)
Cladding anisotropy	**	**

* (α, β) = (mean, standard deviation)

** anisotropy according to ref. 4 with the anisotropy factors YF = 0.5, YH = 0.75 and YG = 0.25

Table 7.2. Reference power history for the fuel pins

Specification	BWR 8x8	BWR 7x7
Heat load, 0-12000 h (W/cm)	(350, 17.5)	(442, 22.1)
Ramp time (h)	1	1
Heat load after the ramp (W/cm)	(440, 22)	(556, 27.8)
Irradiation time after the ramp (h)	500	500
Fast flux at max. power (10^{14} n/cm^{2}s)	(1.5, 0.075)	(1.5, 0.075)
Burn up at the ramp (% FIMA)	2.25	2.14
Outer cladding temperature (°C)	295	295
Outer pressure (MP)	7.1	7.1

In figs. 7.1 and 7.2 it is noted that a comparison between the two designs would yield quite different results for the two failure modes. This stresses the importance of choosing the correct failure mode for the evaluation of different designs. The influence of the ramp rate (the ramp time, fig. 7.1) is much more pronounced for the stress corrosion failure mode than for the overstrain failure mode. This is important when defining reasonable restrictions on reactor operation.

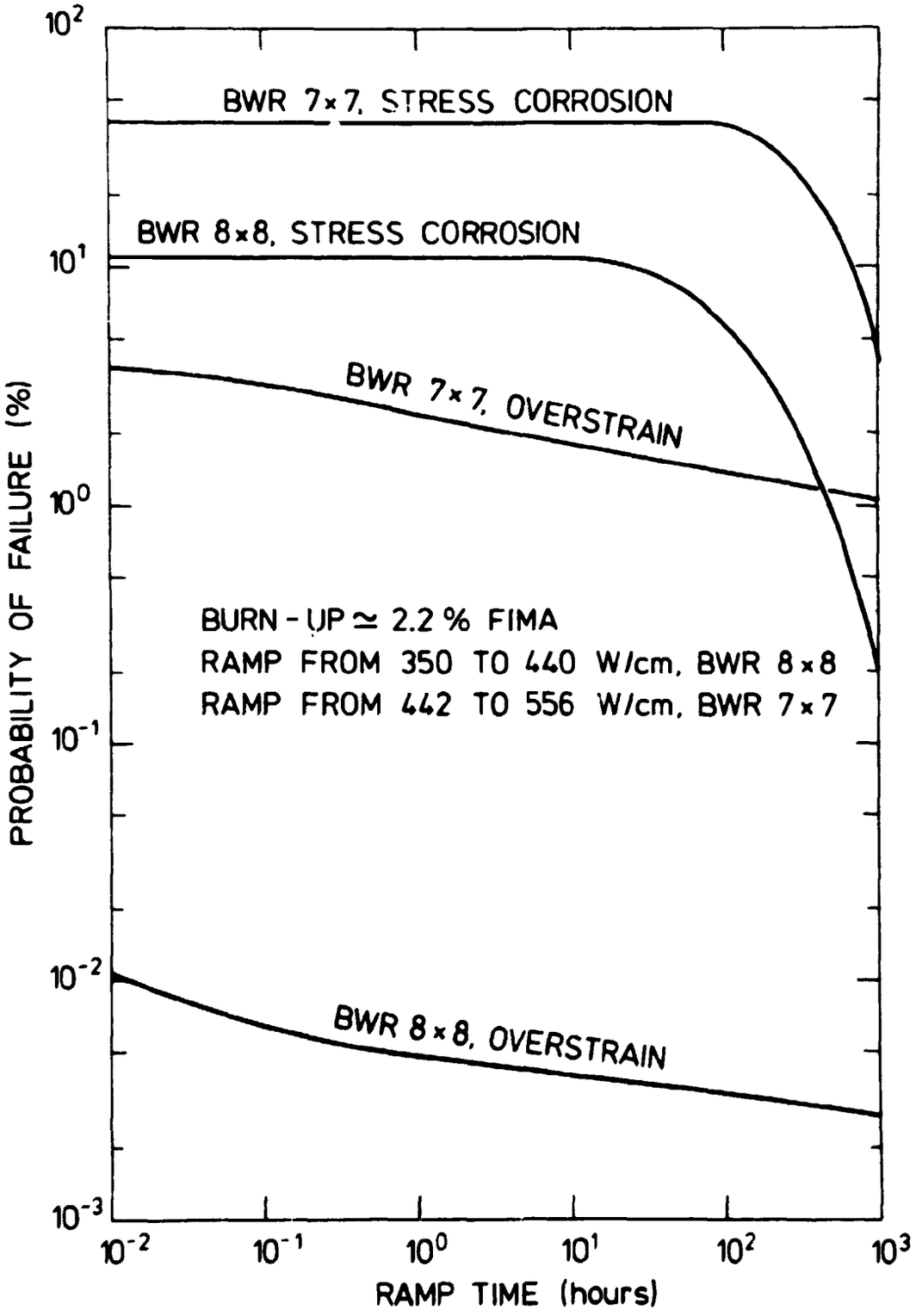

Fig. 7.1. Failure probability for the 7x7 and the 8x8 BWR designs as a function of the ramp rate.

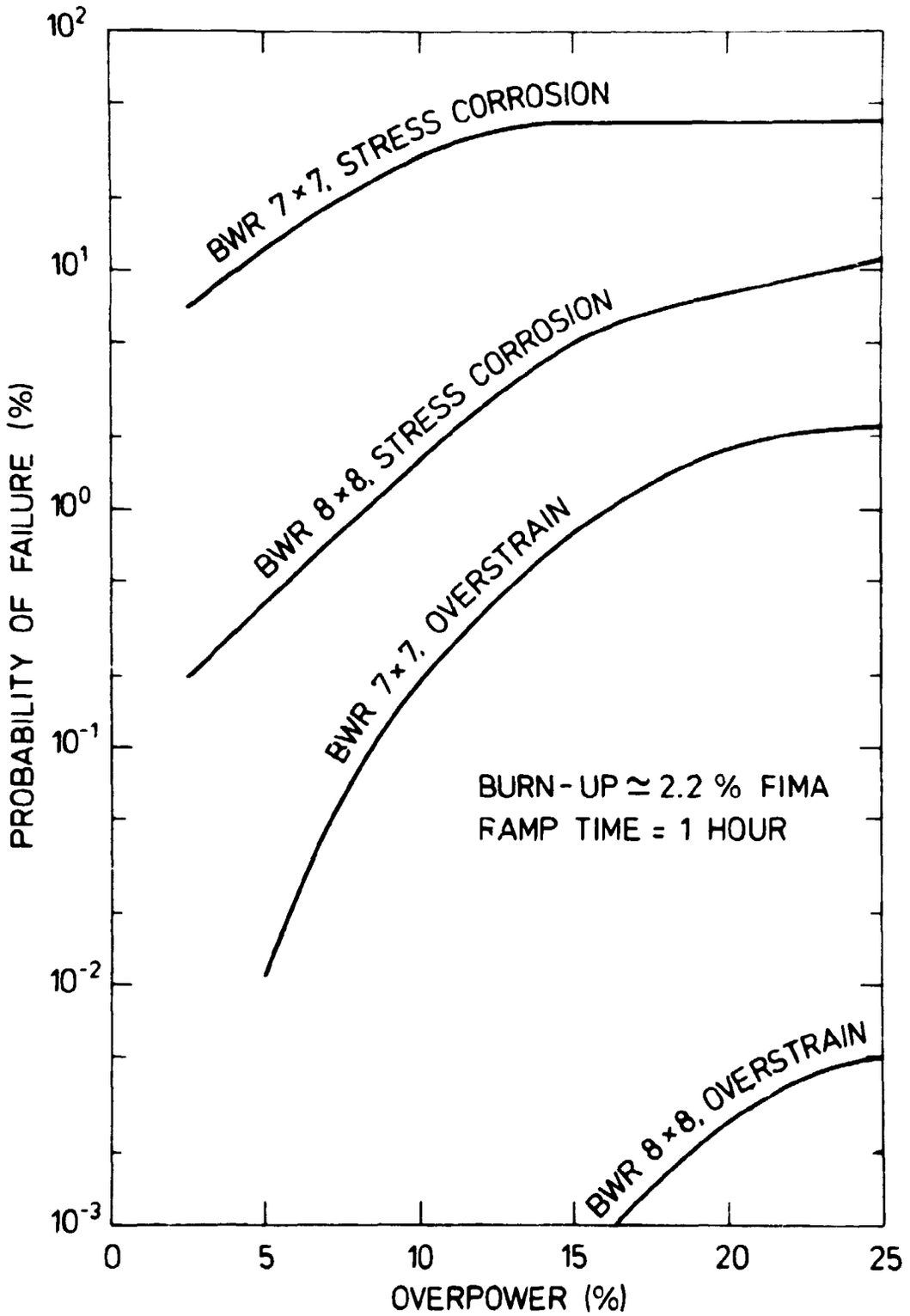

Fig. 7.2. Failure probability for the 7x7 and the 8x8 BWR designs as a function of the overpower in the ramp.

7.2. Influence of the individual design and material parameters

The contribution to the variance of the maximum tangential stress and of the permanent tensile strain (excluding the secondary creep) during the ramp is shown in figs. 7.3 and 7.4 for the 8x8 design. The mean values and the standard deviations as calculated by the Taylor approximation for both stress and strain are in good agreement with the values calculated by the Monte Carlo approximation. The Taylor approximation to the stress corrosion damage stress is poor due to the shape of the pdf. For a fixed ramp rate, the stress corrosion damage is non-linearly correlated with the stress.

As noted in the two figures, the contributions from different material parameters for stress and strain dominate their variance. This again leads to the conclusion that strain alone cannot be used, except under special conditions, to predict the failures caused by stress corrosion. Furthermore, it is observed that manufacturing tolerances have practically no influence on stress or strain at this high level of burnup. The large uncertainty associated with the plenum volume is caused primarily by the uncertainty in the free volume in the pin, and it has very little to do with manufacturing tolerances.

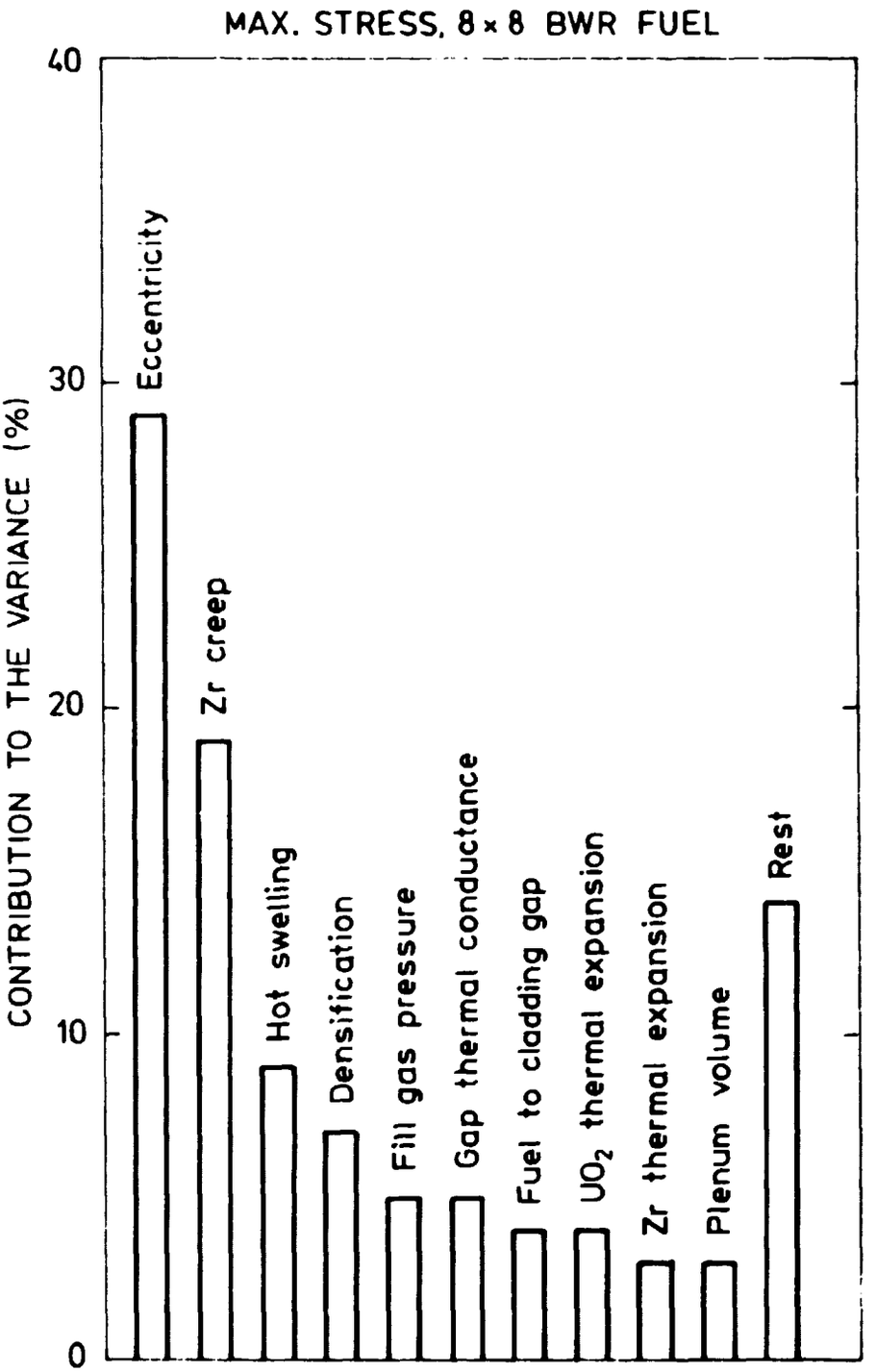

Fig. 7.3. Contribution to the variance of the maximum stress for the 8x8 BWR design.

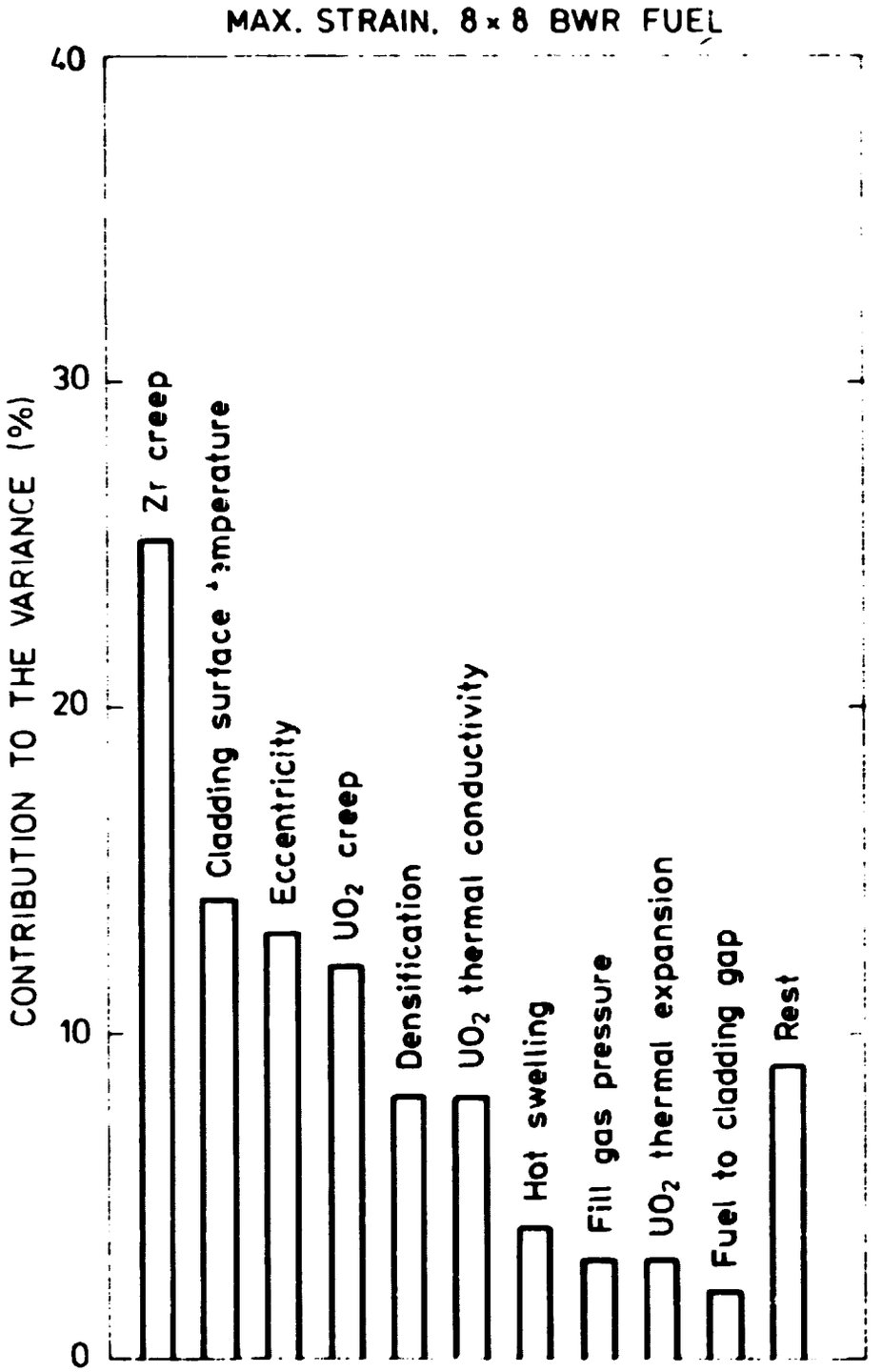

Fig. 7.4. Contribution to the variance of the average tensile strain for the 8x8 BWR design.

8. CONCLUSION

The computer program FRP was developed for the statistical evaluation of nuclear fuel. The statistical methods employed are Monte Carlo simulations and a low-order Taylor approximation. The latter is, for most variables, able to characterize fuel performance with high accuracy; however, for accurate prediction of failure Monte Carlo simulations are necessary.

Calculations performed with the computer code have shown: (a) Stress corrosion failures cannot in general be correlated with the average (or maximum) strain. (b) For constant ramp rate, a correlation between stress corrosion failures and the maximum stress seems possible. (c) The material parameters are dominant (in the considered example) in the contribution to the variance of the stress and the strain; therefore, little improvement in reliability is obtained by decreasing the fabrication tolerances. (d) Efforts should rather be concentrated on obtaining additional information on important material properties such as creep, swelling, fission gas release, gap conductance, etc., thereby decreasing the uncertainty on these parameters.

REFERENCES

1. Hahn, G.J. and Shapiro, S.S. Statistical Models in Engineering (Wiley, New York 1968) 355 pp.
2. Misfeldt, I. Probabilistic Approach to Reliability Predictions for LWR Fuel Rods. Risø-M-1927 (1977) 19 pp.
3. Hasofer, A.M. and Lind, N.C. Exact and Invariant Second-Moment Code Format. ASCE J. Eng. Mech. Div. 100, No. 1 (1974) 111-121.
4. Misfeldt, I. FFRS: A Computer Program for the Thermal and Mechanical Analysis of Fuel Rods. Risø Report No. 373 (1978) 53 pp.
5. Ross, A.M. and Stoute, R.L. Heat Transfer Coefficient between UO_2 and Zircaloy-2. AECL-1552 (1962) 67 pp.
6. Vitanza, C. Private Communication.
7. Andrews, M.G., Freeburn, H.R., and Pati, S.R. Light Water Reactor Fuel Rod Modeling Code Evaluation, Phase II Topical Report. CENPD-218 (1976) 163 pp.
8. Davies, J.H. et al. Irradiation Tests to characterize the PCI Failure Mechanism. NEDO-21551 (1977) 44 pp.
9. McDonald, R.D., Hardy, D.G., and Hunt, C.E.L. Unirradiated UO_2 in Irradiated Zirconium Alloy Cladding. Trans. Am. Nucl. Soc. 17 (1973) 216-217.
10. Davies, J.H. et al. Irradiation Tests to Characterize the PCI Failure Mechanism. NEDO-21551 (1977) 44 pp.
11. Roberts, J.T.A. et al. An SCC Model for Pellet-Cladding Interaction Failures in LWR Fuel Rods. Paper presented at The Fourth International Conference on Zirxonium in the Nuclear Industry, Stratford Hilton, Stratford-upon Avon, England, June 26-29, 1978.
12. Wood, J.C. Factors Affecting Stress Corrosion Cracking of Zircaloy in Iodine Vapour. J. Nucl. Mater. 45 (1972) 105-122.
13. Elayaperumal, K., De, P.K., and Balachandra, J. Stress-Corrosion Cracking of Zircaloy-2 in Methanol-Iodine Solutions. J. Nucl. Mater. 45 (1972) 323-330.

14. Busby, C.C., Tucker, R.P., and McCauley, J.E. Halogen Stress Corrosion Cracking of Zircaloy-4 Tubing. J. Nucl. Mater. 55 (1975) 64-82.
15. Weinberg, J.G. Iodine Stress Corrosion Cracking of Zircaloy-4 Tubing. WAPD-TM-1048 (1974) 23 pp.
16. Garlick, A. Fracture of Zircaloy Cladding under Simulated Power Ramp Condiitions. J. Nucl. Mater. 49 (1974) 209-224.
17. Videm, K. and Lunde, L. Fuel Element Failures Caused by Iodine Stress Corrosion. Ann. Nucl. Energy 3 (1976) 305-313.
18. Misfeldt, I. Material Properties for LWR Fuel Rod Modelling. Risø-M-2117. To be published.
19. Mac Donald, P.E. and Thompson, L.B. (eds.). MATPRO. A Handbook of Materials Properties for Use in the Analysis of Light Water Reactor Fuel Rod Behaviour. ANCR-1263 (1976) 224 pp.
20. Gittus, J.H., Howl, D.A., and Hughes, H. Theoretical Analysis of Cladding Stresses and Strains Produced by Expansion of Cracket Fuel Pellets. Nucl. Appl. Technol. 9 (1970) 40-46.
21 Misfeldt, I. The Reliability of Nuclear Fuel. In: Probabilistic Analysis of Nuclear Reactor Safety. Topical Meeting May 8-10, 1978, Los Angeles, California. Vol. 2 (American Nuclear Society, Hinsdale, Ill., 1978), paper 3.2, 1-12.

APPENDIX A

Specification of the numerical example used in chapter 6

The chosen power history simulates a control rod sequencing in a BWR, when the power is returned to full power immediately after the control rod movements. The considered fuel rod is in a high power position, close to a control rod which was inserted a short period and then withdrawn. For the design data are chosen values typical for BWR fuel.

The power history, the design data and the stochastic variables in the material data are described in the following.

The power as a function of time is shown in fig. A.1.

The uncertainty of the individual pin powers, as calculated by a reactor physics calculation, is at least $\pm$5% ($\pm$ 1 standard deviation). The three power levels (P_1, P_2 and P_3) can be considered as independent. The uncertainties of the fast flux and the outer cladding temperature are assumed to be $\pm$5% ($\pm$ 1 standard deviation) and $\pm$2% ($\pm$ 1 standard deviation) respectively. The power levels, the outer cladding temperature and the fast flux are assumed to follow a normal distribution.

The irradiation conditions (power history) are summarized in table A.1.

The used design data are shown in table A.2. As mean value is used the nominal values, the standard deviations are based on typical tolerances for BWR fuel as specified in ref. 18. All design variables are assumed to be normally distributed.

The material equations used in FRP are described in ref. 18. The mean value, the standard deviation and the distribution type is shown in table A.3 for the stochastic variables in the material equations.

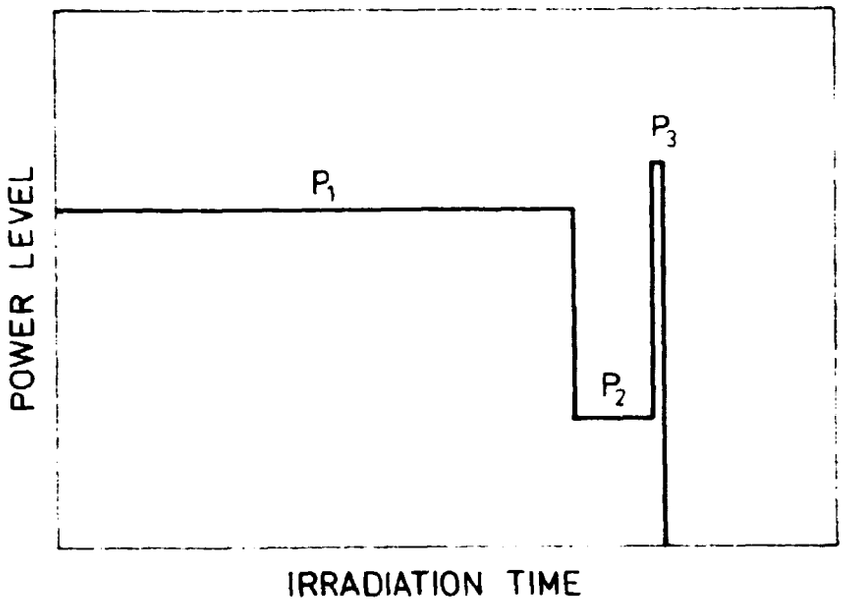

Fig. A.1. Power history for the example.

Table A.1. Power history for the example

period h	power* w/cm	fast flux* 10^{14}n/cm^2 sec	outer cladding temperature* °C
0-24	0-360	0-1.0	295
24-15400	360	1.0	295
15400-15401	360-136	1.0-0.4	295
15401-17630	136	0.4	295
17630-17630.01	136-410	0.4-1.15	295
17630.01-17654	410	1.15	295

*mean values

Table A.2. Design data for the example

Design parameter	Short name	Mean value	Standard deviation	Unit
Inner cladding radius	RCI	5.33	0.0075	mm
Cladding thickness	TCLAD	0.80	0.021	mm
Radial gap	TGAB	0.11	0.011	mm
Density	TDEN	96	0.67	% TD
Equivalent length	LEQ[1)]	3.6	0.72	m
Plenum volume	VP	37.	7.4	cm^3
Fill gas volume	RF	37.	7.4	cm^3
Cladding yield strength at 300°	SIGMAF	300.	15.	MP
Inverse neutron diffusion length	KAPPA	80.	16.	m^{-1}
Average grain size	GRAIN	25.	5.	µm
Cladding surface roughness	RH1	130	26.	µm
Fuel surface roughness	RH2	90	18.	µm
Densification parameter	WEFF[2)]	0.1×10^{-4}	0.035×10^{-4}	

Anisotropy factors[3)]: YF = .5; YH = .75, YG = .25

Porosity distribution: 0.16% porosity with r = 0.1 µm
1.6% porosity with r = 0.6 µm
2.2% porosity with r = 6 µm

1) defined as: LEQ= (fuel stack length) (average pin power)/ (max pin power)

2) parameter in the densification equation, the equation is described in ref. 18.

3) simplified anisotrop theory for permenent deformation, described in ref. 4.

Table A.3. Stochastic variables in the material equations

Material property*	Short name	Distribution**	Mean value	Standard deviation	Unit
Zircaloy thermal conductivity	CO	N	13.5	1.01	W/m
UO_2 thermal expansion	ALFAF	N	1×10^{-5}	0.1×10^{-5}	K^{-1}
Zircaloy thermal expansion	ALFAC	N	0.53×10^{-5}	0.05×10^{-5}	K^{-1}
Youngs modulus, zircaloy	EC	N	7.6×10^{10}	0.5×10^{10}	N/m^2
Mean thermal conductivity of UO_2 and zircaloy	KM	N	6.5	0.98	W/m
A constant in the gap conductance equation	CRS	LN	1.2	0.42	-
Factor in the porosity correction to the UO_2 thermal conductivity	EO	N	2.5	0.5	-
Constant in the UO_2 thermal conductivity	EI	N	8.056	0.3	-
Fission energy	EFIS	N	200	20	MeV
Zircaloy plastic deformation	KMAX	N	1.2×10^{9}	0.12×10^{9}	MP
	DELK	N	-1.4×10^{6}	0.22×10^{6}	MP/K
	NPL	N	0.1	0.012	-
	BFL	N	0.4×10^{-21}	0.08×10^{-21}	cm/n
Zircaloy creep	FCLAD	LN	1.2	0.5	-
UO_2 creep	FUO2	LN	1.7	2.5	-
Solid swelling	KSW	N	0.8	0.08	$FIMA^{-1}$
Hot (gaseous) swelling	KHTS	N	4.75×10^{-3}	1×10^{-3}	$FIMA^{-1}K^{-1}$
	MHTSWL	N	0.1	0.02	-
Poisons ratio, zircaloy	NY	N	0.3	0.07	-
Parameters in FFRS	QREF	N	$20. \times 10^{3}$	$4. \times 10^{3}$	-
	QBURN	N	0.5×10^{-6}	0.1×10^{-6}	-
Stress concentration in the cladding	SIGFAC	N	1.25	0.2	-
Excentricity of the pellet	ECCENT	LN	0.5	0.2	-

* The material equations are described in refs. 4 and 18

** N = normal distribution
LN = lognormal distribution

APPENDIX B

Typical applications of FRP, from reference 21.

The versatility of the code FRP makes it capable of handling quite different situations. Examples of the use are:

1. Irradiation experiments

When preparing and evaluating experiments it is important to know the expected distributions of the results and their sensitivity to uncontrolled parameters and tolerances on the specifications. From numerous ramp experiments it is obvious that the distribution of the experimental results is important. Profit from these experiments is considerably increased by the introduction of probabilistic considerations in the planning as well as in the evaluation of the tests.

In table 2 is shown the 65%, 95% and 99% expection intervals calculated by FRP for the EOL strain, the released fission gas and the maximum temperature for the M20-1B pin.

2. Comparison between designs

Since the reliability is the logical basis for design comparisons, it is necessary to include probabilistic methods in the design comparison. For certain "reference power histories" the reliability as well as the influence from design and material parameters are calculated. These calculations show, besides the difference between the designs, that many of the tolerances specified for the fuel are unnecessarily low, they could be increased without affecting the reliability of the fuel.

Fig. 2 shows a comparison between two standard BWR fuel designs, the design data and the reference power history are specified in table 3. The figure also illustrates the influence of the ramp rate (time to reach full power after changes in the power distribution).

3. Safety related applications

In order to estimate the consequences of some minor, but frequent, accidents leading to local or overall fuel ramps, FRP includes a simple core simulator. The simulator can give the power as a function of time for a number of axial segments in each fuel rod.

The consequences of the following situation have been investigated for a BWR reactor:

At the end of the second cycle (for the fuel elements considered) a control rod is half inserted. After 90 days the control rod is withdrawn at full power. The overall power is assumed to be almost unchanged.

The fuel rods in the four elements nearest to the control rod are divided into 5 groups as shown in fig. 3. The pin power histories, the nodal failure probability and the total number of failed rods assuming the node size to be 10 cm are given in table 4.

The node size of 10 cm corresponds approximately to the size of the test specimens in stress corrosion experiments.

Table 2. Comparison between the experimental data for pin M20-1B and the expected values as calculated by FRP.

Value	experimental results	Calculated by FPP mean	65% expectation intervals	95%	99%
EOL average strain, %	0.35	0.29	0.21-0.38	0.13-0.49	0.05-0.53
Max. temperature, °C	1950	2110	1870-2330	1630-2680	1590-2770
Released fission gas, %	40	36	26-45	15-55	10-65

Table 3. Design data and reference power history for the fuel pins.

Specification	BWR 8x8	BWR 7x7
inner cladding diameter (mm)	(10.8, 0.015)*	(12.42, 0.017)*
cladding thickness (mm)	(0.864, 0.022)*	(0.94, 0.024)*
diametral gap (mm)	(0.228, 0.023)*	(0.30, 0.03)*
density (% af theoretical)	(94.4, 0.66)*	(94.4, 0.66)*
grain size (μm)	(25, 5.0)*	(25, 5.0)*
densification	stable	stable
fill gas/pressure (atm)	1 He	1 He
heat load, 0-8000 h (W/cm)	440	556
heat load, 8000-16000 h (W/cm)	150	193
heat load after the ramp (W/cm)	550	707
fast flux at max. power (n/cm^2)	$1.5x10^{14}$	$1.5x10^{14}$
burn-up at the ramp, % FIMA	2.5	2.5
burn-up at the ramp, MWd/tUO_2	20000	20000

* (mean, standard deviation)

Table 4. Data and consequences for the control rod withdrawl.

Pin group	Heat load, w/cm			P(failure) per node %	Failed pins 0-40 cm axiel location	total
	0-15400 h	-17630h	-17654h			
1	360	125	430	3.3	2.6	3.5
2	365	260	410	3.0	2.9	4.0
3	350	180	390	0.8	1.1	1.3
4	360	320	390	0.24	0.4	0.5
5	310	280	350	0.02	0	0

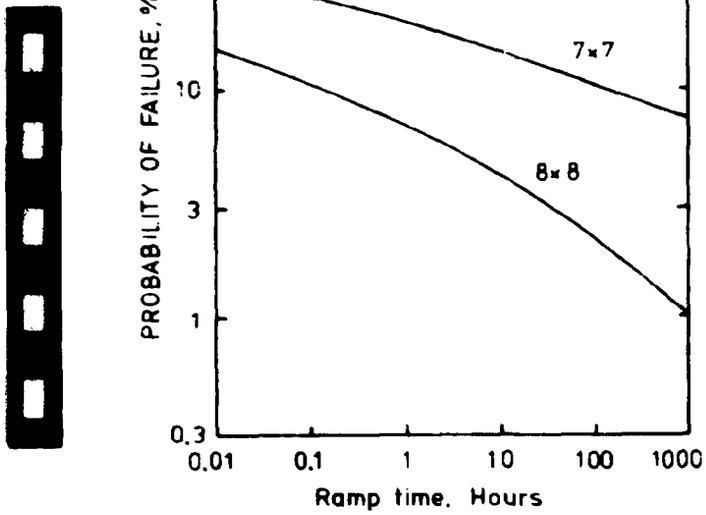

Fig. 2. Failure probability as a function of the ramp rate for two designs.

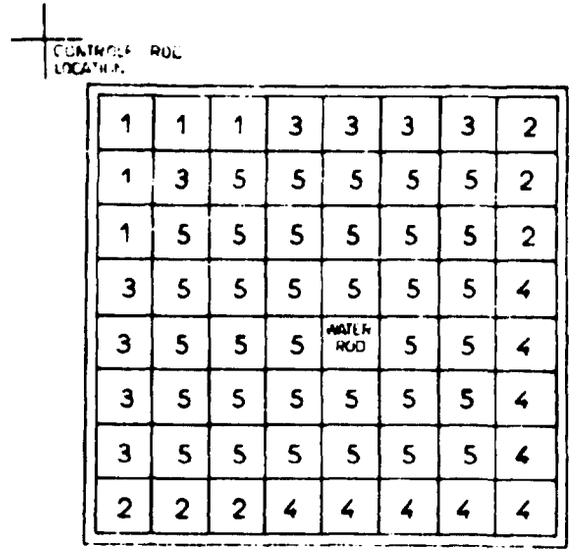

Fig. 3. Pin groups.

Sales distributors:
Jul. Gjellerup, Sølvgade 87,
DK-1307 Copenhagen K, Denmark

Available on exchange from:
Risø Library, Risø National Laboratory,
P. O. Box 49, DK-4000 Roskilde, Denmark

ISBN 87-550-0586-1
ISSN 0418-6443